ACS APPLIED MATERIALS & INTERFACES

www.acsami.org

Research Article

Poly(lactide-*co*-glycolide) Nanoparticles Mediate Sustained Gene Silencing and Improved Biocompatibility of siRNA Delivery Systems in Mouse Lungs after Pulmonary Administration

Lan Wu, Lin-Ping Wu, Jingya Wu, Jin Sun, Zhonggui He, Cristina Rodríguez-Rodríguez, Katayoun Saatchi, Lea Ann Dailey, Urs O. Häfeli, Dongmei Cun,* and Mingshi Yang*

Cite This: *ACS Appl. Mater. Interfaces* 2021, 13, 3722–3737

Read Online

ACCESS | Metrics & More | Article Recommendations | Supporting Information

ABSTRACT: Pulmonary delivery of small interfering RNA (siRNA)-based drugs is promising in treating severe lung disorders characterized by the upregulated expression of disease-causing genes. Previous studies have shown that the sustained siRNA release *in vitro* can be achieved from polymeric matrix nanoparticles based on poly(lactide-*co*-glycolide) (PLGA) loaded with lipoplexes (LPXs) composed of cationic lipid and anionic siRNA (lipid−polymer hybrid nanoparticles, LPNs). Yet, the *in vivo* efficacy, potential for prolonging the pharmacological effect, disposition, and safety of LPNs after pulmonary administration have not been investigated. In this study, siRNA against enhanced green fluorescent protein (EGFP-siRNA) was either assembled with 1,2-dioleoyl-3-trimethylammonium-propane (DOTAP) to form LPX or co-entrapped with DOTAP in PLGA nanoparticles to form LPNs. The disposition and clearance of LPXs and LPNs in mouse lungs were studied after intratracheal administration by using single-photon emission computed tomography/computed tomography (SPECT/CT) and gamma counting. Fluorescence spectroscopy, Western blot, and confocal laser scanning microscopy were used to evaluate the silencing of the EGFP expression mediated by the LPXs and LPNs after intratracheal administration to transgenic mice expressing the EGFP gene. The *in vivo* biocompatibility of LPXs and LPNs was investigated by measuring the cytokine level, total cell counts in bronchoalveolar lavage fluid, and observing the lung tissue histology section. The results showed that the silencing of the EGFP expression mediated by LPNs after pulmonary administration was both prolonged and enhanced as compared to LPXs. This may be attributed to the sustained release characteristics of PLGA, and the prolonged retention in the lung tissue of the colloidally more stable LPNs in comparison to LPXs, as indicated by SPECT/CT. The presence of PLGA effectively alleviated the acute inflammatory effect of cationic lipids to the lungs. This study suggests that PLGA-based LPNs may present an effective formulation strategy to mediate sustained gene silencing effects in the lung *via* pulmonary administration.

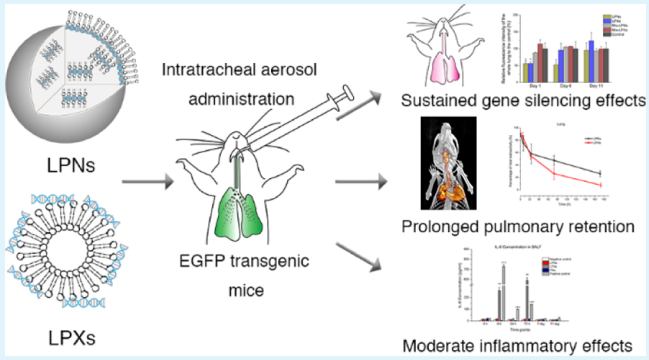

KEYWORDS: *small interfering RNA, poly(lactide-co-glycolide) nanoparticles, cationic lipoplexes, pulmonary delivery, gene silencing, disposition, biocompatibility*

1. INTRODUCTION

Small interfering RNA (siRNA) is short double-stranded RNA that mediates gene silencing by sequence-specific cleavage of mRNA with a complementary sequence *via* the RNA interference (RNAi) pathway.[1,2] Downregulating the expression of disease-causing gene(s) by the treatment with chemically synthesized, exogenous siRNA is a valid means to treat diseases, which has been underlined in 2018 by the first FDA approval of an siRNA-based drug, that is, Alnylam's Patisiran for the treatment of polyneuropathy in patients with hereditary transthyretin-mediated amyloidosis.[3]

Several major challenges must be overcome to realize the full potential of therapeutics based on siRNA, one of them being a clinically applicable delivery solution. Because of the presence of nucleases, siRNA molecules are highly unstable in extracellular biological fluids and must be transfected into the cytosol of target cells before incorporation in the RNA-induced silencing complex. At present, two nonviral approaches are used to deliver siRNA to target cells. The first approach includes the chemical modification of siRNA to protect against degradation and to enhance cell transfection

Received: November 30, 2020
Accepted: December 30, 2020
Published: January 13, 2021

https://dx.doi.org/10.1021/acsami.0c21259
ACS Appl. Mater. Interfaces 2021, 13, 3722–3737

efficiency.[4] The second approach is to formulate siRNA with transfection reagents, for example, lipids, polymers, peptides, and inorganic substances, into nanoscale delivery systems.[5−9] The first commercialized product Patisiran is one of the examples in which siRNA was formulated with lipid excipients into lipid nanoparticles.[10]

Previous studies have demonstrated that many lipids including [(6Z, 9Z, 28Z, 31Z)-heptatriaconta-6,9,28,31-tetraen-19-yl] 4-(dimethylamino) butanoate (DLin-MC3-DMA), lipidoids, and 1,2-dioleoyl-3-trimethylammonium-propane (DOTAP) are effective cellular transfection agents for siRNA delivery.[11−13] In addition, polymeric nanoparticles based on poly(lactide-*co*-glycolide) (PLGA) loaded with lipoplexes (LPXs) could mediate the effective suppression of protein expression by supporting the delivery of siRNA *in vivo*.[14] The PLGA matrix protects the siRNA from degradation during delivery[15] and improves the safety of delivery by reducing the cytotoxic effects of the cationic lipids. Moreover, PLGA could exhibit an extended siRNA release profile *in vitro*.[16] However, it is not clear whether the PLGA would enable an extended gene silencing effect of siRNA *in vivo*, which can be crucial for assessing the potential clinical translation of siRNA therapy using biodegradable PLGA as a delivery system.

Although sometimes overlooked, the lung is an important organ and portal for drug administration. Several studies have shown that pulmonary delivery of siRNA is promising for the treatment of severe lung diseases by silencing disease related genes, for example, the genes of epidermal growth factor receptor or vascular endothelial growth factor to treat lung cancer,[17−19] the genes of the essential subunit of virus to treat airway inflammatory lung disease,[20,21] the genes of epithelial sodium channel to treat cystic fibrosis,[22] the genes of IL-5 and GATA-3 to treat asthma,[23,24] and VCAN gene to treat chronic obstructive pulmonary disease.[25] This can be attributed to the direct deposition of siRNA at the site of the disease, which may result in a more efficient knock-down of specific target genes as compared to other administration routes.

The present study was aimed to investigate the disposition, pharmacological effect, and biocompatibility of intratracheally administered LPXs and LPNs *in vivo* for a period of more than 10 days. siRNA against enhanced green fluorescent protein (EGFP) (EGFP-siRNA) was used as the model drug compound and incorporated into LPXs and LPNs prior to dosing to EGFP transgenic mice *via* four sequential intratracheal administrations to evaluate the gene knockdown efficiency of the nanoparticles. Single-photon emission computed tomography/computed tomography (SPECT/CT) and gamma counting were employed to investigate the lung deposition and clearance of the two formulations. The *in vivo* gene silencing efficiency of these two formulations at each separated part of the lungs at day 1, 6, and 11 after the last dosing was evaluated by measuring the fluorescence intensity of EGFP in the sliced lung tissue and the amount of EGFP by Western blot. The biocompatibility of LPXs and LPNs was evaluated with respect to the pro-inflammatory cytokine level, neutrophil counting, total cell counting, and total protein level in mice bronchoalveolar lavage fluid (BALF). Our results reveal that LPNs exhibited prolonged gene silencing effects, lower systemic absorption, and significantly improved biocompatibility compared to LPXs with the presence of PLGA after pulmonary administration.

2. EXPERIMENTAL SECTION

2.1. Materials. Duplex siRNA directed against EGFP and mismatched siRNA were provided by GenePharma Co. Ltd (Suzhou, Jiangsu, China). For EGFP-siRNA, the sequence of the sense strand was 5′-pACCCUGAAGUUCAUCUGCACCACcg-3′ and the antisense strand sequence was 5′-CGGUGGUGCAGAUGAACUU-CAGGGUCA-3′, where underlined capital letters represent 2′-*O*-methylribonucleotides, lower case letters represent 2′-deoxyribonucleotides and p represents a phosphate residue.[26] For mismatched siRNA, the sequence of the sense strand was 5′-pGGUCCUCGCC-GUCCAACCUAACUAA-3′ and the antisense strand was 5′-UUAGUUAGGUUGGACGGCGAGGACC-3′.

PLGA (molar ratio 75:25, M_W 20 kDa) was purchased from Wako Pure Chemical Industries (Osaka, Japan). DOTAP solubilized in chloroform (25 mg/mL) was purchased from Avanti Polar Lipids (Alabaster, AL, USA). Polyvinyl alcohol (PVA) 403 (80% degree of hydrolysis, viscosity 2.8−3.3 MPa·S) was provided by Kuraray (Osaka, Japan). A Quant-iT RiboGreen RNA reagent kit was purchased from Invitrogen-ThermoFisher Scientific (Paisley, UK). *N*-Octyl-*β*-D-glucopyranoside (OG) and lipopolysaccharide (LPS) were purchased from Sigma-Aldrich (St. Louis, MO, USA). The BCA protein level analysis kit was purchased from Beyotime Biotechnology Co. Ltd (Shanghai, China). Heparin sodium salt (H123383 ≥ 180 U/mg) was purchased from Aladdin Industrial Corporation (Shanghai, China). Mouse IL-6, TNF-*α*, IL-1*β*, IFN-*γ*, and IL-4 ELISA kits were purchased from BOSTER Biological Technology Co. Ltd (Wuhan, China). Wright−Giemsa staining reagent was provided by Beijing Solarbio Science & Technology Co. Ltd (Beijing, China). All buffer were prepared using RNase-free diethyl pyrocarbonate (DEPC) treated water. Additional chemicals, unless otherwise stated, were purchased from local companies at the analytical grade.

2.2. Preparation of siRNA-Loaded Nanoparticles. The LPXs composed of siRNA and DOTAP were prepared by mixing DOTAP dispersion with siRNA solution at different N/P ratios (the ratio of the number of amine groups in DOTAP to the number of phosphate groups in the siRNA). The thin-film hydration method was used to facilitate the dispersion of DOTAP in buffer.[13,27] In this study, 1.08 mL of DOTAP chloroform solution (25 mg/mL) was added to a round bottom flask, and a thin dry film of DOTAP was prepared by evaporating the chloroform with a rotary evaporator (RE-200A, Shanghai Yarong Biochemical Factory, Shanghai, China). The film was hydrated for 30 min with 1.5 mL of 10 mM *N*-(2-hydroxyethyl)piperazine-*N*′-ethanesulfonic acid buffer (pH 7.4) and then sonicated three times, 1 min for each time and with 10 min pause at an input power of 200 W to reduce the average particle size. Subsequently, equal volumes of DOTAP dispersion and siRNA solution were mixed at designed N/P ratios (62, 10, and 5) and vortexed for 5 min to formulate LPXs.

The siRNA-loaded LPNs were prepared by the double emulsion solvent evaporation method with minor changes.[28] siRNA solution (125 *μ*L) served as the inner water phase (W_1), a solution of 2.25 mg of DOTAP and 12.75 mg of PLGA in 250 *μ*L of dichloromethane (DCM) served as the oil phase (O). The two phases were mixed and sonicated with an ultrasonic processor (650-92, Biosafer Co. Ltd, Nanjing, China) for 2 min to prepare the primary W_1/O emulsion. Subsequently, 4 mL of 2% (w/v) PVA in DEPC-treated water was mixed with the primary emulsion and sonicated again to form a secondary W_1/O/W_2 emulsion. LPNs were formed by solidified emulsion droplets after the evaporation of DCM. The LPNs were collected by centrifugation at 13,600*g* for 10 min, washed three times with RNase-free DEPC-treated water, and re-dispersed in medium appropriate for the subsequent experiments. Pure PLGA nanoparticles (PNs) were prepared according to the same process without the addition of DOTAP.

2.3. Characterization of siRNA-Loaded Nanoparticles. The LPXs and LPNs were characterized with respect to intensity-weighted mean hydrodynamic diameter (*z*-average), polydispersity index (PDI), zeta-potential, encapsulation efficiency (EE), and siRNA loading. The LPN suspension and LPXs were diluted 100 times with

https://dx.doi.org/10.1021/acsami.0c21259
ACS Appl. Mater. Interfaces 2021, 13, 3722−3737

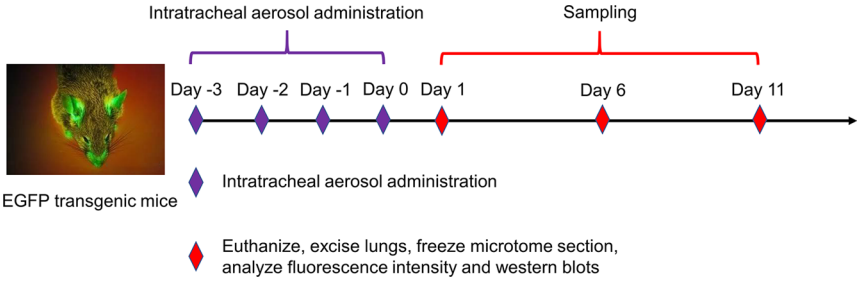

Figure 1. Design of animal experiments.

RNase-free DEPC-treated water before measuring the particle size and zeta potential with a Malvern Zetasizer Nano ZS 90 (Malvern Instruments, Worcestershire, UK) at 25 °C. Three batches of formulations were measured (N = 3), and each measurement was repeated three times (n = 3).

The EE of siRNA in LPNs was determined by using a published procedure[16] with minor modification. In brief, the siRNA entrapped in the LPNs was extracted with 500 μL of the so-called HD solution (containing heparin with a concentration of 1 mg/mL and OG with a concentration of 100 mM) after the complete dissolving of 1 mg of LPNs in 300 μL of chloroform. The extracted siRNA was quantified by using the RiboGreen RNA reagent kit according to the manufacturer's instruction.

The EE of siRNA in the LPXs was evaluated by determining the concentration of un-complexed siRNA using the RiboGreen RNA reagent kit without adding of the HD solution. This analytic procedure was validated by comparing the measured siRNA concentration in the same LPX sample with or without HD solution. The data for method validation were shown in the Supporting Information.

2.4. Cell Culture. The human lung adenocarcinoma cell line A549 stably expressing EGFP (A549-EGFP cell line, acquired from Obio Technology Corp., Ltd. Shanghai, China) was used for the investigation of the gene silencing efficiency of the LPXs and LPNs *in vitro*. The details of cell line establishment are illustrated in Supporting Information Section A3. The cells were cultured in F-12K medium (Hyclone, GE Healthcare Life sciences Co.Ltd, Germany) containing 10% fetal bovine serum (Gibco, life technologies), 1% penicillin and streptomycin (P/S) (both from Sigma-Aldrich Co. Ltd, St. Louis, MO, USA), and 2 μg/mL of puromycin (Abcam Co. Ltd, Cambridge, UK).

2.5. *In Vitro* Gene Silencing Efficiency and Cell Viability Assays. The A549-EGFP cells were seeded into 24-well tissue culture plates (Corning Co. Ltd, NY, USA) at a density of 6×10^4 cells/well. After 24 h of growth (30% confluence), the culture medium was replaced with one of the following transfection agents: (1) the LPXs, LPNs, mismatched siRNA LPXs (Mis-LPXs), or mismatched siRNA LPN (Mis-LPNs) suspension in serum-free F-12K medium with 20, 40, 80, or 120 nM siRNA concentration in individual wells; (2) the mixture of 1 μL of Lipofectamine 2000 (Invitrogen, Ltd. Paisley, UK) and EGFP-siRNA (40 nM of final concentration) for the positive control and referred to as EGFP-siRNA + lipo 2000 group; (3) the mixture of 1 μL of Lipofectamine 2000 and mismatched siRNA (40 nM of final concentration) and referred to as the mismatched siRNA + lipo 2000 group; (4) EGFP-siRNA solution (40 nM); or (5) cell culture medium for the negative control group. After 8 h of incubation, the medium was removed and the cells were washed twice with 1 mL of pH 7.4 phosphate-buffered saline (PBS, Sigma-Aldrich) and further cultured in 1 mL of full medium for another 40 h. The cells were then collected for flow cytometry. Three wells of negative control cells were fixed via incubating with 3.7% (w/w) paraformaldehyde for 15 min at room temperature to kill all the cells and served as the control for the cell viability study. All of the collected cells were stained with 200 μL of 1 μg/mL propidium iodide (PI, Invitrogen Ltd., Paisley, UK) solution.

The expression of EGFP in cells was evaluated by using a flow cytometer (MACS Quant Analyzer flow cytometer, Miltenyi Biotec, Teterow, Germany) and the data were analyzed using MACSQuantify software (Miltenyi Biotec). Representative peaks and gating strategies are provided in Supporting Information Figure S9. The gene silencing effects of different formulations were calculated by dividing the green fluorescence intensity of A549-EGFP cells treated by that of untreated negative control cells. The viability of cells was calculated according to eq 1 below, where $PI_{treated\ cells}$ was the fluorescence intensity of PI of treated cells and $PI_{fixed\ cells}$ was the fluorescence intensity of PI of fixed cells because only the dead cells could be stained with PI.

$$\text{Cell viability (\%)} = \left(1 - \frac{PI_{treated\ cells}}{PI_{fixed\ cells}}\right) \times 100\% \quad (1)$$

2.6. *In Vivo* Gene Silencing Activity of LPXs and LPNs in EGFP Transgenic Mouse Lungs. EGFP transgenic mice bred from Jackson's lab with the genotype of C57BL/6-Tg (CAG-EGFP) were purchased from Shanghai Biomodel Organism Science & Technology Development Co., Ltd., (Shanghai, China). All animal experiments were performed in accordance with animal care guidelines approved by the Life Science Research Center and Ethical Committee of Shenyang Pharmaceutical University (SPU). All the animals were allowed a week of acclimatization period before the experiment. The genotype of animals was checked before the *in vivo* study (Supporting Information Figure S6).

The formulations of the LPXs or LPNs with an N/P ratio of 10 were used to evaluate their gene silencing efficiency *in vivo*. A total of 45 EGFP gene positive mice with a comparable level of the EGFP gene expression were divided into five groups randomly, that is, the LPX group, the LPN group, Mis-LPX group, Mis-LPN group, and control group, nine mice for each group. Test samples (25 μL) containing 0.3 nmol (5 μg) per dose of siRNA for the LPX, LPN, Mis-LPX, and Mis-LPN groups, and 25 μL of PBS for the control group were nebulized with a hand-hold aerosolizer (HRH-MAG4, Yuyan instruments Co. Ltd., China)[29] and administered directly into the trachea of the mice once a day and repeated for four sequential days. At day 1, 6, and 11 after the last administration, three mice from each group were euthanized (Figure 1). The lungs were excised and divided into five anatomical lung lobes (left lung, superior lobe of the right lung, middle lobe of the right lung, inferior lobe of the right lung, and post-caval lobe). The expression of EGFP in each segment of the whole lung was evaluated by measuring the fluorescence intensity of EGFP in tissue sections with confocal laser scanning microscopy (CLSM, LSM 710, Carl Zeiss Microimaging GmbH, Jena, Germany) and fluorescence microplate reader (Varioskan flash, Thermo Scientific Co. Ltd, Rockford, IL, USA). Besides, the EGFP protein levels were quantified by Western blot analysis. The gene silencing efficiencies of formulations *in vivo* were investigated relative to the expression of EGFP in the lungs from the control group.

2.6.1. Fluorescence Intensity of EGFP Quantitatively Measured by Fluorescence Spectroscopy. Small pieces of the tissue were taken from the middle of each segment of lung and lysed with 100 μL of RIPA cell and tissue lysis buffer added with phenylmethylsulfonyl fluoride and protease inhibitor. The protein concentration in lysis samples was quantified with a BCA kit according to the manufacturer's instruction, and the fluorescence intensity of EGFP

https://dx.doi.org/10.1021/acsami.0c21259
ACS Appl. Mater. Interfaces 2021, 13, 3722−3737

of the corresponding samples was read with a microplate reader at an excitation wavelength of 494 nm and an emission wavelength of 518 nm.

Because a good linear correlation relationship between the fluorescence intensity and total protein concentration was demonstrated, as shown in the Supporting Information (Figure S8), the determined fluorescence intensity values were always normalized by the samples' total protein amount to eliminate errors because of the individual tissue sample weight difference.[30,31] In addition, a related study indicated that the tissue autofluorescence is not likely to interrupt with the fluorescence intensity results (Figure S7). The normalized fluorescence intensity of each lobe was recorded as FI_n^{number} and FI_{total}^{number} was the weighted average of FI^{number} of five different lobes of the same lung which was calculated according to eq 2 below, where FI_1^{number}, FI_2^{number}, FI_3^{number}, FI_4^{number}, and FI_5^{number} are the fluorescence intensity of the left lung, superior lobe of the right lung, middle lobe of the right lung, inferior lobe of the right lung, and post-caval lobe, respectively, W_1, W_2, W_3, W_4, and W_5 are the weights of the lung lobes, respectively.

$$FI_{total}^{number} = \frac{FI_1^{number}W_1 + FI_2^{number}W_2 + FI_3^{number}W_3 + FI_4^{number}W_4 + FI_5^{number}W_5}{W_1 + W_2 + W_3 + W_4 + W_5} \quad (2)$$

2.6.2. Western Blot Analysis. A specific volume of the lung tissue lysis sample acquired according to the same method mentioned in Section 2.6.1, corresponding to 10 μg of protein, was separated on 12% sodium dodecyl sulfate-polyacrylamide gel electrophoresis gels and transferred to nitrocellulose membranes. The membrane was blocked using 5% nonfat dry milk and incubated with the primary antibody to EGFP (clone F56-6A1.2.3, mouse monoclonal IgG2b, 1:1000 dilution, Invitrogen Ltd. Paisley, UK) and primary antibody to β-actin (IgM, 1:1000 dilution, Proteintech Group Inc. USA). Chemiluminescence signals were detected with horseradish peroxidase-conjugated secondary antibody (goat anti-mouse IgG, 3:10,000 dilution, cwbiotech, China) and ECL agent (ECL Plus Western Blotting Detection Reagents, GE Healthcare, Belgium). The images were processed with gray level analysis using ImageJ software (https://imagej.nih.gov/ij/, NIH, WA, USA). The gray level of each EGFP strip was divided by the gray level of the corresponding β-actin strip. The total gray level of Western blot of each mouse (WB_{total}) was calculated according to eq 3 below, where WB_1, WB_2, WB_3, WB_4, and WB_5 are the gray level of Western blot of the left lung, superior lobe of the right lung, middle lobe of the right lung, inferior lobe of the right lung, and post-caval lobe, respectively; W_1, W_2, W_3, W_4, and W_5 are the weights of the lung lobes, respectively.

$$WB_{total} = \frac{WB_1W_1 + WB_2W_2 + WB_3W_3 + WB_4W_4 + WB_5W_5}{W_1 + W_2 + W_3 + W_4 + W_5} \quad (3)$$

2.6.3. EGFP Fluorescence Intensity of Lung Sections Observed with CLSM. The lung tissues from different lobes of the excised lungs were sliced into 5 μm thin sections with a cryo-microtome (Leica CM1950, Leica Mikrosysteme Vertrieb GmbH Mikroskopie und Histologie, Germany) and stained with 5 μL of a 10 μg/mL solution of 4′,6-diamidino-2-phenylindol (DAPI, Invitrogen Ltd. Paisley, UK) for 3 min at room temperature, then washed five times with PBS to remove excessive DAPI. The fluorescence of EGFP and DAPI was excited by lasers at 488 and 364 nm wavelengths, respectively. All settings of CLSM including laser intensity, pinhole, and detector gain were kept constant for optimal comparison. The fluorescence intensity of EGFP in the images was converted into numbers by using the RGB measurement with ImageJ software. The measured fluorescence intensity of each lobe was recorded as FI_n^{CLSM} and FI_{total}^{CLSM} was the weighted average of FI of five different lobes of the same lung. The FI_{total}^{CLSM} was calculated according to eq 4 below, where FI_1^{CLSM}, FI_2^{CLSM}, FI_3^{CLSM}, FI_4^{CLSM}, and FI_5^{CLSM} are the fluorescence intensity of the left lung, superior lobe of the right lung, middle lobe of the right lung, inferior lobe of the right lung, and post-caval lobe, respectively, W_1, W_2, W_3, W_4, and W_5 are the weights of the lung lobes, respectively.

$$FI_{total}^{CLSM} = \frac{FI_1^{CLSM}W_1 + FI_2^{CLSM}W_2 + FI_3^{CLSM}W_3 + FI_4^{CLSM}W_4 + FI_5^{CLSM}W_5}{W_1 + W_2 + W_3 + W_4 + W_5} \quad (4)$$

2.7. Evaluation of Long-Term Pulmonary Retention Time, Clearance Rate, and Biodistribution of LPXs and LPNs by SPECT/CT. The retention time, clearance rate, and biodistribution of LPXs and LPNs in mouse lungs after intratracheal administration was evaluated quantitatively by radiolabeling the LPXs and LPNs with ^{111}In and detecting their lung retention using a SPECT/CT technique. The radiolabeling procedure and properties are presented in the Supporting Information in detail.

The imaging studies were conducted at The University of British Columbia (UBC) and performed in accordance with the Canadian Council on Animal Care (CCAC). The protocols were approved by the Animal Care Committee (ACC) of UBC (A16-0150). Five-to six-weeks old healthy female C57BL/6 mice were purchased from Charles River. Mice were allocated into two groups of three individuals. The mice were dosed by intratracheal administration of 25 μL of ^{111}In-LPNs or ^{111}In-LPXs containing 11.1 MBq of ^{111}In, respectively, with the siRNA dosage of 5 μg. At predetermined time points (0, 6, 24 h, 3, and 7 days after administration), SPECT/CT scans were performed using a VECTor/CT preclinical small animal scanner (MILabs, Utrecht, The Netherlands). The details of SPECT/CT scanning and reconstruction are provided in the Supporting Information Section A12. The radioactivity in lungs were calculated by adding 3D volumes of interest (VOIs) in Amide software (V.1.0.4).[32]

For the biodistribution study, 3D VOIs of major related organs (i.e., trachea and mouth, liver, kidney, spleen, stomach, intestine, and bladder) were also drawn and their radioactivity was calculated. On day 11 after the administration, all mice were euthanized and their blood, heart, liver, kidneys, lungs, small intestine, brain, bladder, muscle, spleen, bone, pancreas, feces, and stomach were collected and weighted. The radioactivity of each organ was measured using a gamma counter (Packard Cobra II Autogamma counter, PerkinElmer, Waltham, MA, USA). All the radioactivity at different time points were decay corrected. More details about the calculation are provided in the Supporting Information. The remaining percentage of radioactivity in the lungs was plotted as a function of the time to compare LPXs and LPNs clearance from the lungs.

2.8. *In Vivo* Biocompatibility of LPXs and LPNs after Intratracheal Administration. The experiment was conducted at SPU. Healthy female C57BL/6 mice (5 to 6-weeks old) were purchased from the Laboratory Animal Center of SPU and allocated into 5 groups with 18 mice in each group randomly, that is, the LPNs, LPXs, PNs, positive control, and negative control groups. The mice were dosed with 25 μL of the LPN suspension, LPX suspension, PN suspension, LPS solution, or PBS, respectively, by intratracheal aerosol administration as described before. All the formulations were dispersed in the sterile PBS solution (pH 7.4). The solid concentration was 30 μg/μL (30 mg/kg for a 25 g mouse) for LPNs and PNs; the concentration of DOTAP in the LPN and LPX suspensions was 4.5 μg/μL (4.5 mg/kg for a 25 g mouse); the concentration of LPS was 2 μg/μL; and the siRNA dosage of LPNs and LPXs was 5 μg. All formulations for the *in vivo* study were endotoxin free. LPS was used as a positive control to induce acute inflammatory response to mouse lungs in this study, and PBS was used as a negative control. At each predetermined time points of 0, 6, 24, 72 h, and 7, 11 days after administration, three mice from each group were euthanized. The right bronchi of the mouse lung was ligated with sutures and the left lung was lavaged three times with 1 mL of PBS. The BALF was stored on ice. The right lobes of mice were excised and immersed in 10% formalin for 48 h for tissue fixation.

The collected BALF was centrifuged at 1000*g* for 10 min at 4 °C and the obtained cell pellet was re-suspended in 1 mL of PBS buffer (pH 7.4) for total and differential cell counts for the proportion of

https://dx.doi.org/10.1021/acsami.0c21259
ACS Appl. Mater. Interfaces 2021, 13, 3722−3737

Table 1. Particle Size, Zeta Potential, and EE of siRNA-Loaded Nanoparticles (Mean ± SD, N = 3, n = 3)

nanoparticles	N/P ratio	particle size (nm)	PDI	zeta potential (mV)	EE (%)	actual loading (μg siRNA/mg nanoparticles)	theoretical loading (μg siRNA/mg nanoparticles)
LPNs	62	246.3 ± 1.4	0.09 ± 0.01	37.7 ± 1.9	45.5 ± 5.3	0.5 ± 0.1	1.1
	10	239.3 ± 1.5	0.12 ± 0.01	34.2 ± 0.7	53.6 ± 4.2	3.7 ± 0.3	6.8
	5	233.7 ± 2.1	0.10 ± 0.01	36.7 ± 0.2	51.2 ± 2.6	7.0 ± 0.4	13.7
LPXs	62	153.8 ± 32.6	0.19 ± 0.01	42.3 ± 4.7	101.2 ± 0.6	7.4 ± 0.1	7.3
	10	166.5 ± 10.2	0.22 ± 0.01	46.7 ± 3.9	103.5 ± 1.8	47.2 ± 0.8	45.4
	5	172.0 ± 3.0	0.22 ± 0.09	41.2 ± 2.3	100.6 ± 2.1	91.8 ± 2.0	91.2

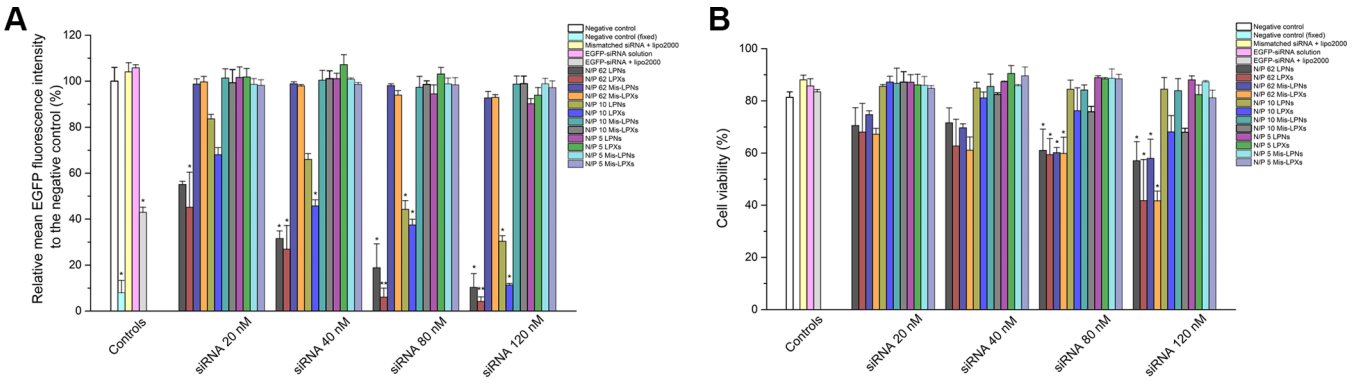

Figure 2. *In vitro* gene silencing efficiency and cell viability of A549-EGFP cells treated with the LPXs and LPNs (bars represent mean values ± SD, n = 3). Percentage of fluorescence intensity of EGFP expressed in A549-EGFP cells after being treated with formulations with different N/P ratios relative to the blank medium treated negative control (A). Cell viability of A549-EGFP cells after being treated with formulations with different N/P ratios (B). The cell viability of negative control (fixed) was 0. Statistical difference studies were conducted relative to the negative control, $^{*}P \leq 0.05$, $^{**}P \leq 0.01$, and $^{***}P \leq 0.001$.

eosinophils, macrophages, and neutrophils after Wright-Giemsa staining. The concentrations of inflammation-related cytokines IL-6 and TNF-α in BALF were determined with sandwich ELISA kits according to the manufacturer's instruction.

Tissue histology was performed on the right lung after dehydrating through ascending gradience of alcohol and embedded in paraffin wax. The sliced sections with a thickness of 5 μm were stained by hematoxylin and eosin stain to assess general morphology with light microscopy (IX71, Olympus, Japan).

2.9. Statistical Analysis. Statistical analyses were performed using the software SPSS (Version 20). The statistically significant differences were conducted with one-way analysis of variance (ANOVA) and independent t-test. P values of less than 0.05 were considered to be significant. The results are reported as mean ± standard deviation (SD).

3. RESULTS AND DISCUSSION

3.1. Physicochemical Characterization, *In Vitro* Gene Silencing Effects, and Cell Viability of LPXs and LPNs. The sizes of LPNs were between 230 and 250 nm and showed a slight increase with an increase in the N/P ratio (Table 1). The size distribution of LPNs was very narrow with a PDI of approx. 0.1. Compared to LPNs, LPXs possessed a smaller particle size, this might be attributed to the absence of PLGA, which made up the bulk volume of the LPNs. Although the zeta potential of LPNs was less positive than LPXs, the positive charge of DOTAP in LPNs was not completely shielded by PLGA. The EE of the LPXs was evaluated by determining the concentration of siRNA in the aliquots of the same LPX samples with or without the presence of HD. Because the RiboGreen RNA reagent could not associate with entrapped siRNA to excite fluorescence, the absence of the HD solution (which could di-associate siRNA from the LPXs) will ensure that the detected fluorescence is proportional to the concentration of free siRNA. The validation of the method was described in the Supporting Information (Table S1). As shown in Table 1, the EEs of the LPXs were nearly 100% at all tested N/P ratios, which could be attributed to the excessive DOTAP in the formulations. A relevant study on the effect of endogenous anionic molecule hyaluronic acid (HA) on the gene silencing performances of LPNs and LPXs proved that the negative impact of HA on the gene silencing effects of LPNs was moderate than on the LPXs because of the presence of PLGA (Figures S2 and S3).

The A549-EGFP cell line was used to assess the *in vitro* gene silencing effect and cytotoxicity of LPXs and LPNs. The cells fixed with paraformaldehyde were all killed and served as the 100% cell death control in the cell viability study. Predictably, the *in vitro* gene silencing efficiency and cytotoxicity induced by LPXs and LPNs varied upon the N/P ratios and the concentrations of siRNA used. The suppressions of EGFP by the LPXs were 0, 32, and 55% at a siRNA concentration of 20 nM; 0, 55, and 74% at the siRNA concentration of 40 nM; 0, 63, and 94% at a siRNA concentration of 80 nM; and 6, 89, and 96% at a siRNA concentration of 120 nM, when the N/P ratios of the formulations were 5, 10, and 62, respectively (Figure 2A). For LPNs, the suppressions of EGFP were 0, 17, and 45% at a siRNA concentration of 20 nM; 0, 35, and 68% at a siRNA concentration of 40 nM; 6, 55, and 81% at a siRNA concentration of 80 nM; and 10, 70, and 90% at a siRNA concentration of 120 nM, when the N/P ratios of the formulations were 5, 10, and 62, respectively (Figure 2A). The results exhibited that the higher the N/P ratio, the higher the efficiency of gene silencing when the concentration of siRNA of LPNs and LPXs was kept the same, which can be attributed to the high concentration of cationic lipid leading to enhanced cell surface binding and subsequent cellular internalization of siRNA.[33] Compared to LPNs at the same N/P ratio and

https://dx.doi.org/10.1021/acsami.0c21259
ACS Appl. Mater. Interfaces 2021, 13, 3722−3737

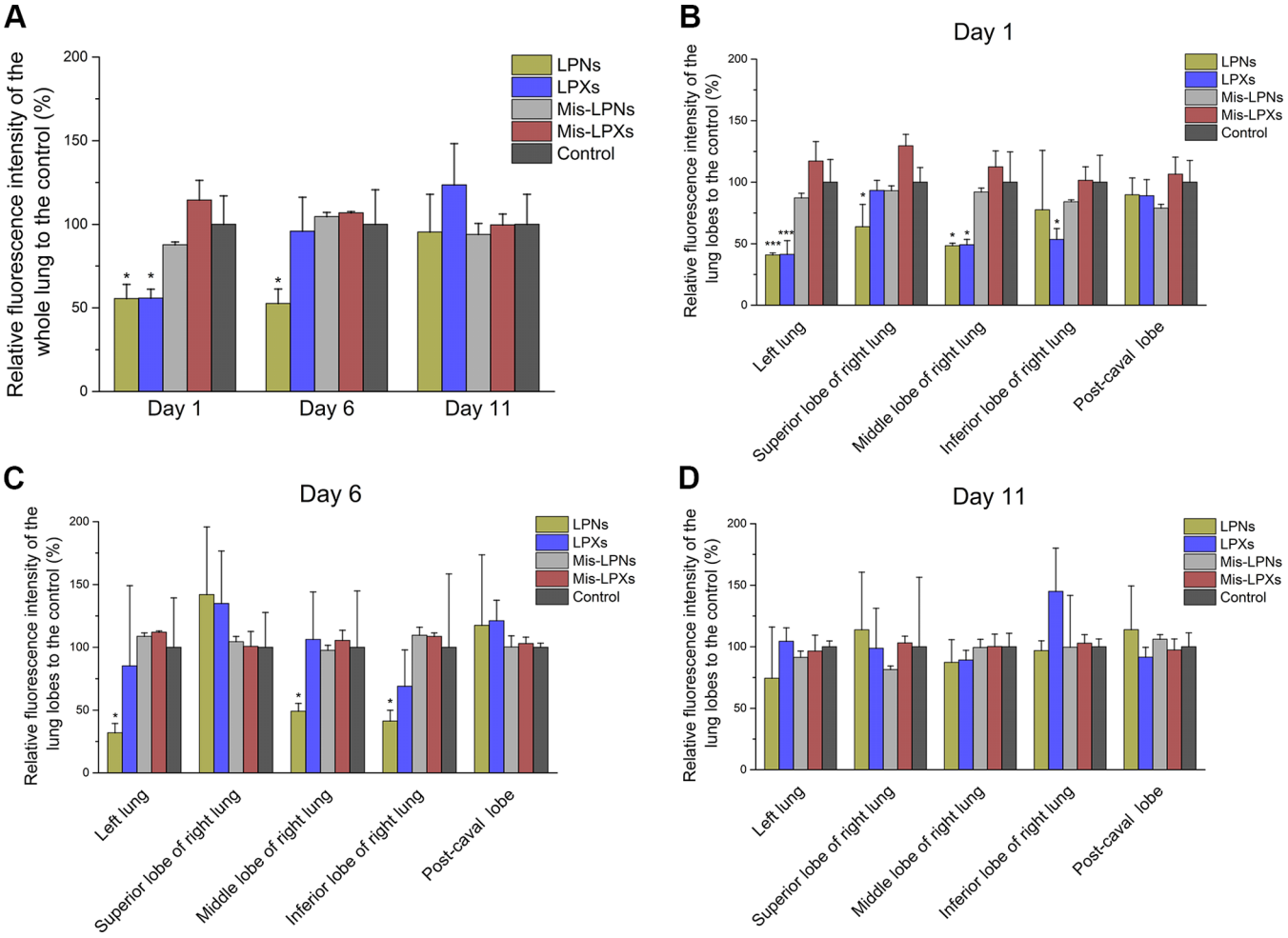

Figure 3. *In vivo* gene silencing effects of the nanoparticles evaluated based on fluorescence spectroscopy (bars represent mean values ± SD, $n = 3$). The fluorescence intensity of EGFP in mouse lungs treated with the nanoparticles relative to the PBS-treated control on day 1, 6, and 11 after the last administration (A). Fluorescence intensity of EGFP in mouse lungs treated with the nanoparticles relative to the PBS-treated control in each lung lobe on day 1 (B), day 6 (C), and day 11 (D) after the last administration. Significant difference in the fluorescence intensity levels of formulation-treated groups were compared with the PBS-treated negative control. *$P \leq 0.05$, **$P \leq 0.01$, and ***$P \leq 0.001$.

siRNA concentration, the enhanced gene silencing efficiency of LPXs may partly be because of the smaller size and higher zeta potential of LPXs, which could facilitate the interaction with the cell membrane and endosomal escape.[34,35]

Despite the higher gene silencing efficiency being achieved, the higher N/P ratio also led to lower cell viability when the concentration of siRNA of LPNs and LPXs was kept the same (Figure 2B). The viabilities of A549-EGFP cells after being treated with the LPXs were 86, 87, and 68% at a siRNA concentration of 20 nM; 90, 81, 62% at a siRNA concentration of 40 nM; 88, 76, and 59% at a siRNA concentration of 80 nM; and 82, 68, and 42% at a siRNA concentration of 120 nM, when the N/P ratios of the formulations were 5, 10, and 62, respectively. For the LPN-treated group, the cell viabilities were 87, 86, and 71% at a siRNA concentration of 20 nM; 87, 85, and 72% at a siRNA concentration of 40 nM; 89, 84, and 61% at a siRNA concentration of 80 nM; and 88, 84, and 57% at a siRNA concentration of 120 nM, when the N/P ratios of the formulations were 5, 10, and 62, respectively. The results showed that the cytotoxicity of the cationic lipid could be circumvented to some extent by the presence of PLGA as a matrix.[16] The EE and loading of siRNA in LPNs were lower than that of LPXs. In order to ensure the same siRNA concentration in each well, higher amounts of LPNs were needed. Despite higher amounts of LPNs being added in the medium, the LPN-treated group still exhibited better cell viability than LPXs, which indicated the excellent biocompatibility of PLGA *in vitro*.

As shown in Figure 2, Mis-LPNs and Mis-LPXs exhibited negligible gene silencing effects (Figure 2A) and similar cell viability as the corresponding EGFP-siRNA-loaded formulations with the same N/P ratio and the concentration of siRNA (Figure 2B). It indicates that the gene silencing effects of EGFP-siRNA-loaded formulations are attributed to the sequence-specific gene silencing effects of EGFP-siRNA, and the off-target effects of these formulations are negligible. The formulations with a N/P ratio of 62 possessed low cell viability, while the formulations with a N/P ratio of 5 exhibited compromised gene silencing efficiency. Therefore, LPNs and LPXs with a N/P ratio of 10 were used for further *in vivo* studies.

3.2. LPNs Mediated Sustained Gene Silencing Effects in the Lung after Intratracheal Administration. EGFP-siRNA is a well-established model compound to study the cellular transfection efficiency of different delivery systems *in vitro* settings.[36] It has also been used as a model siRNA to

https://dx.doi.org/10.1021/acsami.0c21259
ACS Appl. Mater. Interfaces 2021, 13, 3722−3737

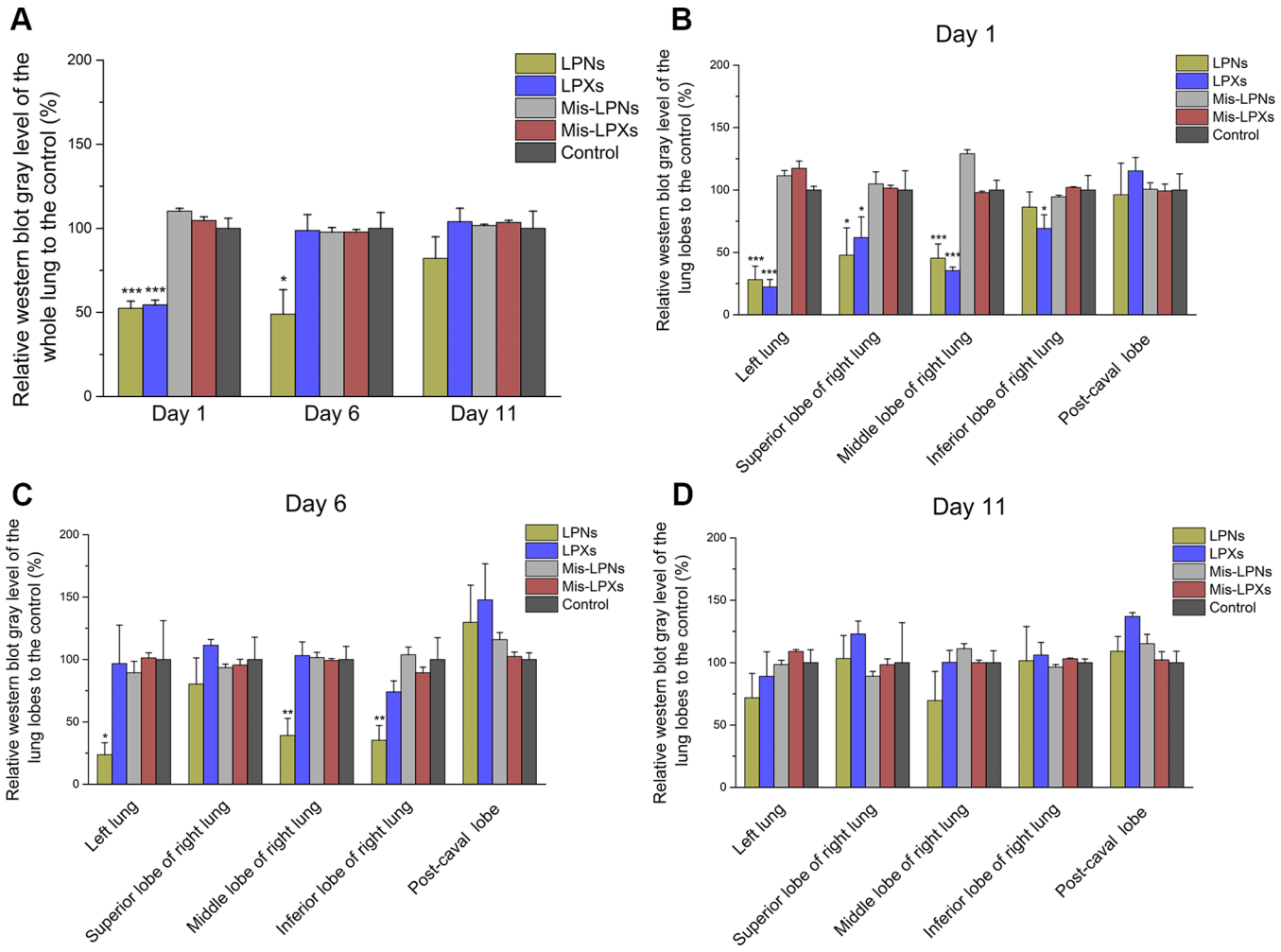

Figure 4. *In vivo* gene silencing effects of the nanoparticles evaluated by Western blot (bars represent mean values ± SD, $n = 3$). Percentage of the total gray level of Western blot images of the EGFP protein extracted from mouse lungs treated with the nanoparticles relative to the PBS-treated control on day 1, 6, and 11 after the last administration (A) and percentage of the gray level of Western blot images of the EGFP protein extracted from mouse lungs treated with the nanoparticles relative to the PBS-treated control in each lung lobe on day 1 (B), 6 (C), and 11 (D) after the last administration. Significant difference in the percentage of the gray level of Western blot images of EGFP protein extracted from mouse lungs of formulation-treated groups were compared with the PBS-treated negative control. $^{*}P \leq 0.05$, $^{**}P \leq 0.01$, $^{***}P \leq 0.001$.

evaluate gene silencing effects in rodents *via* intratracheal administration.[37] Different from previous studies, in this work, we investigated the potential prolonged gene silencing effects of EGFP-siRNA-loaded LPNs in EGFP transgenic mouse lungs after intratracheal administration.

The total fluorescence intensity of the overall lungs was calculated according to the formula presented in the Section 2.6, and the results were presented in Figure 3A. The suppression of EGFP by the formulations was also investigated by using Western blot (Figure 4A). The typical Western blot images are provided in Supporting Information (Figure S10). According to the total fluorescence intensity study, when treated with LPXs and LPNs, EGFP levels in the lung tissues were knocked down by 45% on day 1. While the knockdown efficiency of EGFP by the LPNs was maintained at the same level, that is, about 45%, on day 6, the expression of EGFP in the LPX group returned to the control group levels. The results of Western blot also confirmed these findings, where the gene knockdown percentage by LPXs and LPNs were measured as 46 and 48%, respectively, on day 1, the gene knockdown effects of LPNs on day 6 was similar to that on day 1, that is, approx. 51%, whereas the expression of EGFP in the mouse lungs treated with LPXs returned to the same level as the control group. On day 11, EGFP levels in LPX- and LPN-treated animals returned to the baseline level of the control group.

Total fluorescence intensities from the representative CLSM images of the overall lungs were calculated (Figure 5A) using the formula presented in Section 2.6. The fluorescence intensities of different lobes were extracted from CLSM images of a single sliced tissue from each lobe with the aid of ImageJ software. Although the results can only be indicative but not quantitative, similar information as the quantitative results from the fluorescence study and Western blot analysis can be drawn, that is, the gene silencing effect of LPNs was prolonged compared with LPXs. To give some representative examples of the CLSM images used for the analysis, tissues from the left lung obtained from the formulation-treated groups and control group on day 1, 6, and 11 are presented in Figure 5E−G, respectively. All the CLSM images were presented in the Supporting Information Figure S11.

The results from the three applied methods all suggested that the LPNs exhibit a more efficient *in vivo* gene silencing effect than LPXs. A related study investigating the gene silencing effects of chitosan/anti-EGFP siRNA nanoparticles in

https://dx.doi.org/10.1021/acsami.0c21259
ACS Appl. Mater. Interfaces 2021, 13, 3722−3737

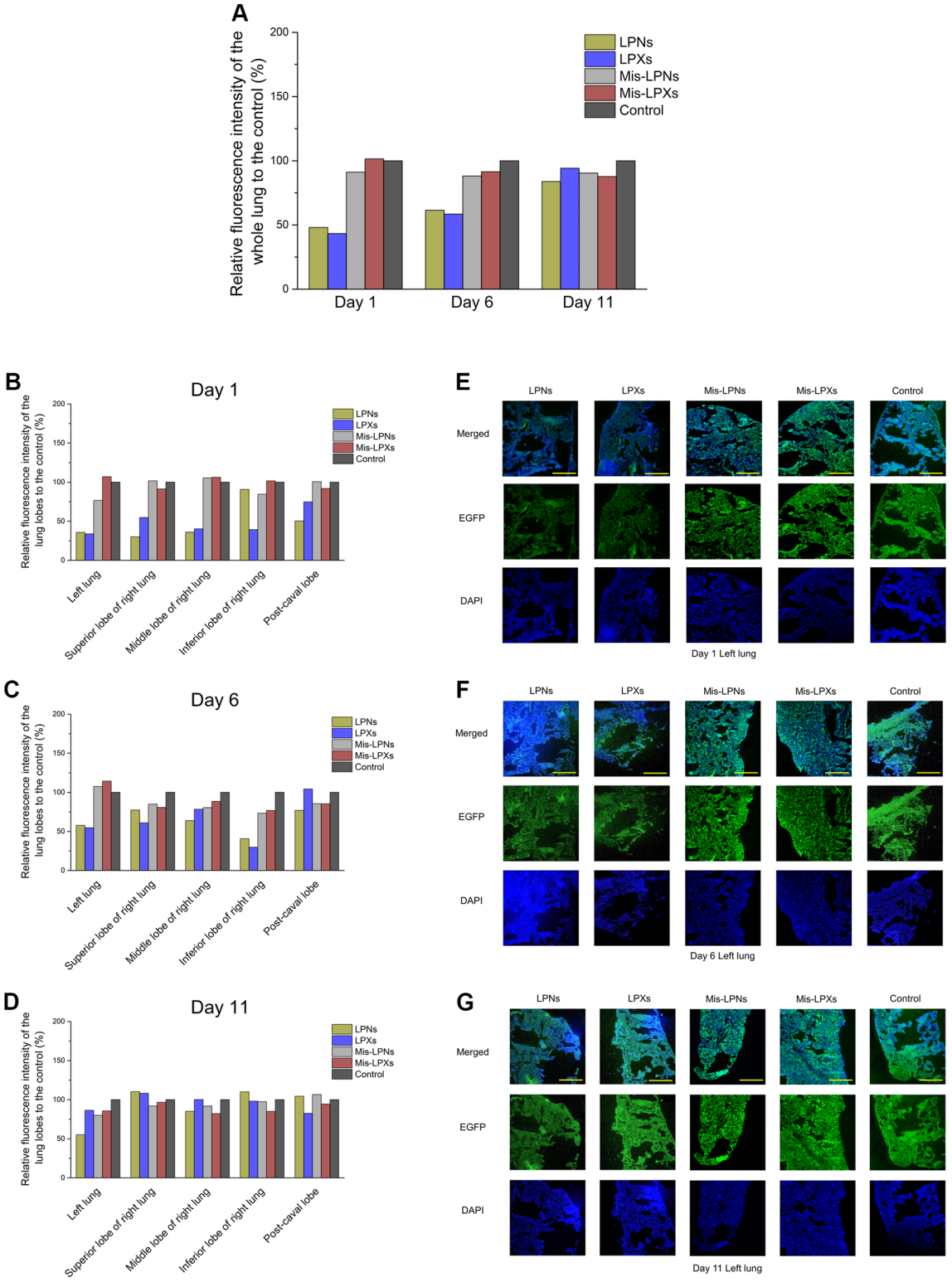

Figure 5. *In vivo* gene silencing effects of the nanoparticles evaluated based on CLSM images. Total fluorescence intensity obtained from CLSM images of mice lung tissues on day 1, 6, and 11 after the last administration (A) and fluorescence intensity obtained from CLSM images of each mice lung lobes on day 1 (B), 6 (C), and 11 (D) after the last administration. Representative CLSM images of mouse left lung lobes on day 1 (E), 6 (F), and 11 (G) after the last administration (scale bar = 200 μm).

EGFP transgenic mouse lungs showed 68% of the gene silencing effect on day 5 after dosing 0.26 μg of siRNA on day 1 and day 3.[38] The N/P ratio that the research group used were 23, whereas it was 10 in our case. In another study, 35 μg of anti-EGFP siRNA formulated with PEG-modified PEI (M_w = 8.3 kDa) at a N/P ratio of 6 exhibited 65% of gene silencing effects in EGFP transgenic mouse lungs on day 5 after intratracheal instillation; however, 58% of EGFP knockdown was also found in nonspecific siRNA against the luciferase GL3 (siCL3)-treated group, which revealed significant off-target

https://dx.doi.org/10.1021/acsami.0c21259
ACS Appl. Mater. Interfaces 2021, 13, 3722−3737

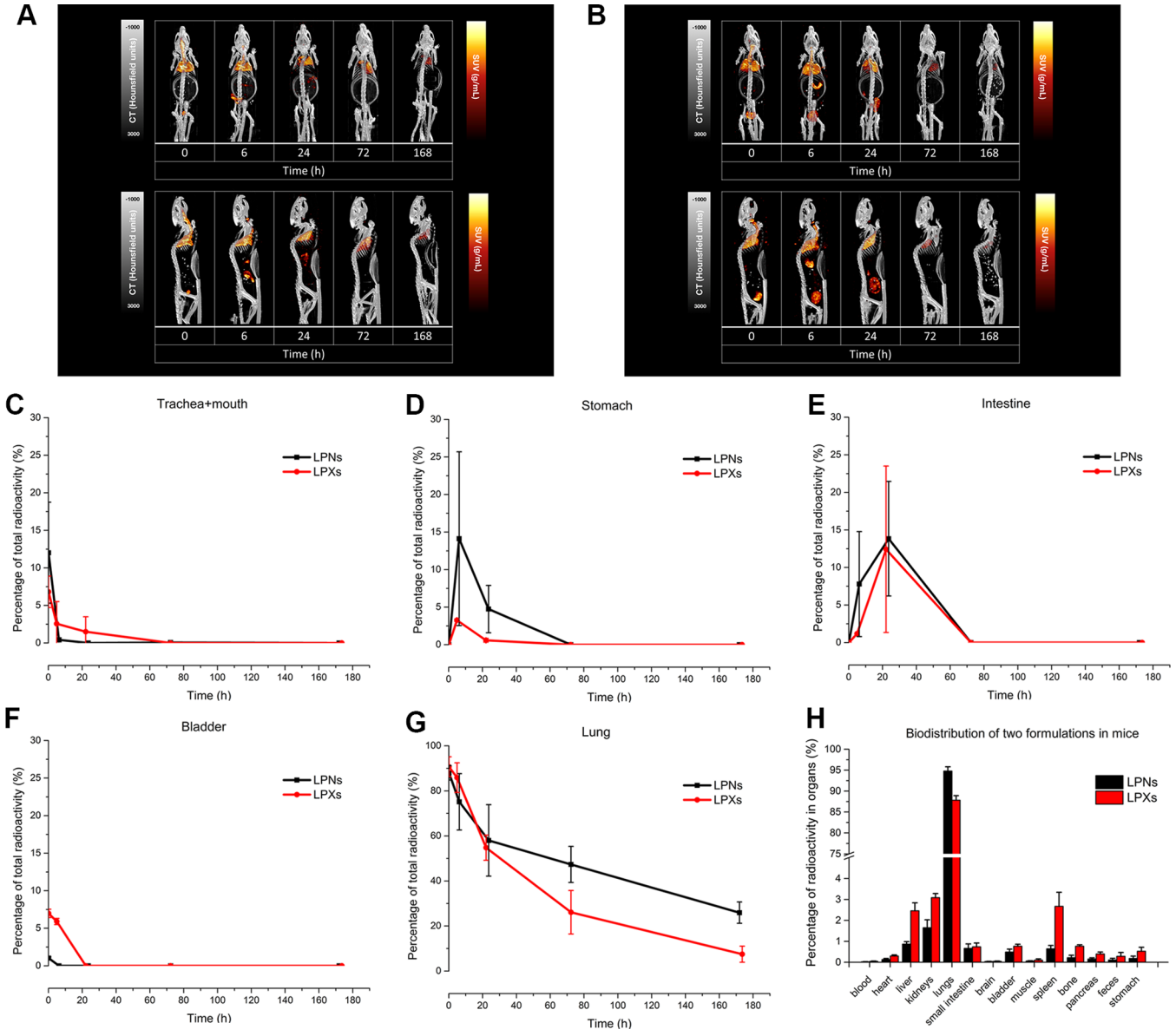

Figure 6. Biodistribution of LPNs and LPXs after intratracheal administration. Respective whole-body SPECT/CT images of ^{111}In-radiolabeled LPNs (A) and respective whole-body SPECT/CT images of ^{111}In-radiolabeled LPXs (B); the animals were monitored up to 7 days after administration. Distribution of LPNs and LPXs in the main organs from 0 h to seventh day after intratracheal administration, investigated by 3D VOI calculation in SPECT/CT images (n = 3) (C−G); whole body biodistribution of LPNs and LPXs at the terminal end point (eleventh day after intratracheal administration), investigated by gamma counting (H).

effects induced by the delivery system. The high nonspecific gene silencing effects can be attributed to the severe inflammatory and immunomodulatory response as well as high biomembrane damage caused by PEI.[7]

In contrast, in the current study, we used a lower dose of siRNA (i.e., 5 μg per dose) and lower N/P ratio (i.e., 10), exhibited moderate but prolonged gene silencing effects with negligible off-target effects. The prolonged suppression of EGFP in the mouse lungs induced by the LPNs as compared to the LPXs might be partially attributed to the sustained-release characteristics of siRNA from LPNs. In the *in vitro* release study, RiboGreen RNA reagent kit was used to determine the concentration of siRNA released from LPNs (Supporting Information Figure S1). It was known that only free siRNA can bind to RiboGreen RNA reagent to exert fluorescence, while the bounded form of siRNA cannot bind to RiboGreen RNA reagent to exhibit detectable fluorescence.[39] To set the siRNA free from the bounded form, HD solution composed of 1 mg/mL of heparin and 100 mM OG was used to dissociate the nanocomplexes. Heparin is a commonly used reagent for the decomplexation of siRNA from LPXs or polyplexes.[33,40] OG is a surfactant, which contributes to the decomplexation of LPXs or polyplexes. In the spiking experiment (Supporting Information Table S1), it was proved that the addition of the HD solution in the LPX suspension could make all siRNA (including free and bounded siRNA) free to bind to RiboGreen RNA reagent to exert fluorescence. Without HD solution, only the fraction of released siRNA in free form could be detected. Therefore, the difference of fluorescence intensity with and without the HD solution can represent the amount of bound siRNA and free siRNA in the medium. As shown in the Supporting Information Figure S1,

https://dx.doi.org/10.1021/acsami.0c21259
ACS Appl. Mater. Interfaces 2021, 13, 3722−3737

intensive fluorescence signals could be observed from the release medium with the presence of the HD solution, while negligible a fluorescence signal could be detected without the addition of the HD solution. It indicates that the majority of siRNA released from LPNs was in the form of bound siRNA instead of free siRNA, which is in accordance with an earlier study.[16] The PLGA matrix mediated a sustained release profile of bound siRNA from the LPNs. These sustained-release characteristics of siRNA from LPNs *in vitro* might have also happened *in vivo*, contributing to the prolonged suppression of EGFP in the mouse lungs.

While overall gene silencing effects in the whole mouse lungs were the sum of those in different lobes and confirmed by three different methods (see Figures 3A, 4A, and 5A), the levels of the suppression of EGFP in the different lung lobes induced by the same formulation varied significantly (see Figures 3B−D, 4B−D, and 5−D). In general, the suppression of EGFP was significantly more profound in the left lung lobes, followed by the middle lobes of the right lungs. The superior lobes of the right lungs and the inferior lobes of the right lungs showed smaller gene silencing effects, while the post-caval lobes in all animals showed almost no gene suppression. One reason behind the variation in the efficacy in different lung lobes may be attributed to the variation in the amount of deposited formulations in different lung lobes owing to the anatomy of mouse lungs. The entry of the left lung lobe is larger than that of the middle lobe of the right lung, then followed by the superior lobe of the right lung and the inferior lobe of the right lung.[41] Other studies have also reported the uneven deposition of the formulations in different lung lobes after intratracheal administration.[42,43] In addition, our previous study suggested that the administration methods would also influence the distribution of formulations within different lung lobes.[44]

The positive charge and nanosize of LPNs and LPXs promoted their *in vivo* gene silencing performances.[45] However, while LPXs exhibited better *in vitro* gene silencing performance than LPNs, similar performance of the two nanoparticle formulations were observed *in vivo* on day 1 and better performance of LPNs were observed *in vivo* on day 6. This can be attributed to the different experiment settings that were employed in the *in vitro* and *in vivo* studies, including the duration of the experiments and microenvironment. The *in vitro* gene silencing performance of the nanoparticles were evaluated after 8 h of the incubation with cells. The better *in vitro* gene silencing performance of LPXs than LPNs could be attributed to the better cellular uptake of LPXs as compared to LPNs in the *in vitro* study (Supporting Information Figure S5). However, the *in vivo* microenvironment is deemed to be more complex than that in the *in vitro* experiment setting. The results from the preliminary colloidal stability study suggest that LPXs are more prone to aggregation than LPNs (Supporting Information Figure S4). It can be postulated that the difference in this colloidal stability will alter their gene silencing performance *in vivo* as compared to that *in vitro*.

3.3. LPNs Exhibited Prolonged Pulmonary Retention and Decreased Systemic Absorption Compared with LPXs after Intratracheal Administration. In the present study, LPXs and LPNs were radiolabeled by ^{111}In with the radiolabeling efficiencies of 84.9 and 98.6% (Supporting Information Figure S12), respectively. The ^{111}In was labeled onto the PE and mixed with DOTAP before formulating into LPNs or LPXs; therefore, it can be postulated that ^{111}In are localized both in the core and shell of the LPNs. In LPXs, however, ^{111}In might have been dispersed in the nanoparticles together with DOTAP. The radiolabeling procedure resulted in negligible change in the particle size, PDI, and zeta potential of LPXs and LPNs as compared to the formulations before radiolabeling (Supporting Information Table S2). After intratracheal aerosol administration, LPXs and LPNs had a similarly high deposition in the lung (i.e., 88 and 91%, respectively), as shown in Figure 6G. After 11 days, ca. 2% of the initial LPXs remained in the lung, compared to ca. 25% of the initial LPNs which were retained in the lung. The clearance rate of LPNs from the lung was much slower than that of LPXs. The results revealed that in addition to the sustained release characteristics of LPNs imposed by PLGA, an extended retention of LPNs versus LPXs in mouse lungs might partially contribute to the prolonged pharmacological effect of LPNs. A recent paper, where quantitative fluorescence imaging tomography was used to detect the *in vivo* process of LPNs and LPXs loaded with Alexa Fluor 750-labeled siRNA for 24 h, also reported prolonged lung retention after the intratracheal administration of siRNA-loaded LPNs over LPXs, which correlates with their *in vitro* release profile that LPNs exhibit better colloidal stability than LPXs.[46] This is in line with what we observed in the SPECT/CT imaging study and our *in vitro* study (Supporting Information Figure S4). The different clearance rates of LPXs and LPNs might be related to their varied surface chemistry, which might have resulted in different rates of phagocytosis and clearance by the lung macrophages.[47−49] In addition, the different particle size might also contribute to different pulmonary clearance rates.[50,51] The exact mechanism behind the extended retention of the LPNs over LPXs in the lung warrants further investigation, nonetheless, our study suggests that the superior pharmacological effect of the LPNs over LPXs can be attributed to an extended retention of the LPNs in the lung.

To investigate the disposition of the formulations after intratracheal administration, trachea and mouth, liver, kidney, spleen, stomach, intestine, and bladder were chosen as 3D VOIs for semi-quantitative analysis. LPNs had higher accumulation in trachea and mouth as compared to LPXs at 0 h and disappeared at 72 h. The signals of both LPXs and LPNs appeared in the stomach at 6 h, with LPNs' signal being higher. The signals decreased at 24 h and disappeared at 72 h. LPNs and LPXs started to appear in the intestine at 6 h after intratracheal administration, reached peak value at 24 h, and disappeared at 72 h. The appearance of the signals in the gastrointestinal tract was likely related to the mucociliary clearance and subsequent swallowing, which were reported to be the major clearance mechanism of the formulations deposited in the upper respiratory tract.[52,53] However, the ingested dose was eliminated gradually and nearly undetectable after 72 h, which indicated that the mucociliary clearance did not dominate for LPNs and LPXs after 72 h. LPX-treated group showed much higher radioactivity in the bladder than the LPN-treated group, and the radioactivity of LPXs in the bladder disappeared at 24 h. In contrast, the radioactivity of LPNs in the bladder disappeared at 6 h. The radioactivity in the bladders can be attributed to free isotopes, that is, ^{111}In in this case.

No radioactivity was detected in the liver, kidneys, spleen, or blood during the 3D imaging analysis. Nevertheless, at the terminal end point on day 11, when gamma counting, an analytical method with higher sensitivity than 3D imaging

https://dx.doi.org/10.1021/acsami.0c21259
ACS Appl. Mater. Interfaces 2021, 13, 3722−3737

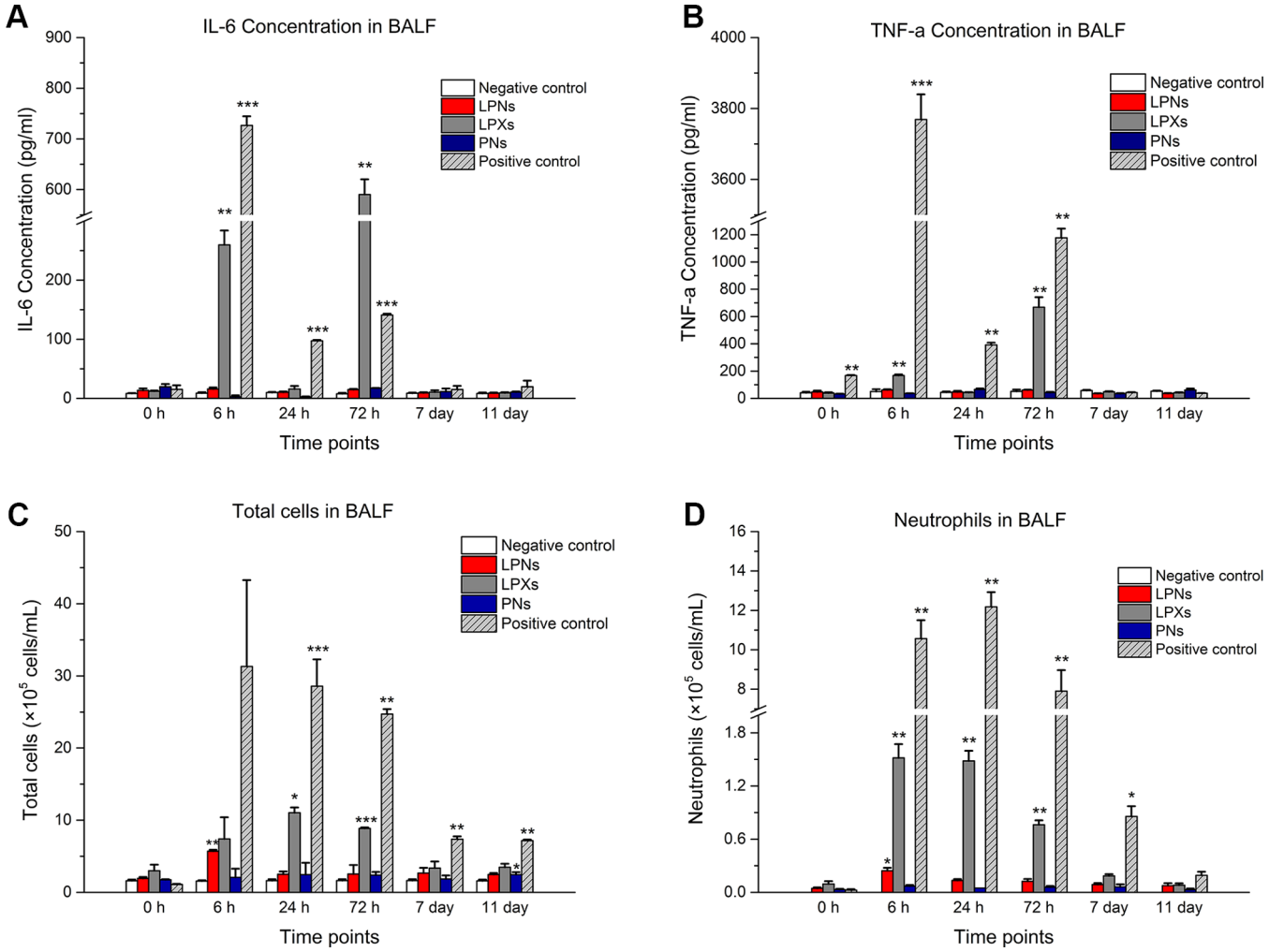

Figure 7. Assessment of cytokine levels and cell levels in BALF. (A) IL-6 concentration in BALF. (B) TNF-α concentration in BALF. (C) Total number of cells in BALF. (D) Neutrophils in BALF. Column represent mean ± SD (n = 3). Significant difference in the cytokine levels and cell levels were compared with the PBS treated negative control: *$P \leqslant 0.05$, **P $\leqslant$ 0.01, and ***P $\leqslant$ 0.001.

analysis, was applied to measure the biodistribution of the formulations, radioactivity was detected within these organs. The results show that the accumulation of LPXs in the liver, kidneys, and spleen was higher than that of LPNs (Figure 6H). In addition, 94.8 and 87.8% of the total remaining reactivity of LPNs and LPXs, respectively, in the body are from the lung. It suggests that the majority of LPNs and LPXs remained in the lung throughout the study and the systemic absorption of LPNs and LPXs were not significant, supporting that the sustained gene silencing effect of LPNs in the lung is attributed to its extended retention in the lung.

It should be noted that the siRNA could show different biodistribution patterns from that of ^{111}In-labeled nanoparticles formulations. After all, ^{111}In was labeled to chelator-linked PE and mixed with DOTAP prior to formulating with the siRNA into the LPXs and LPNs, rather than being labeled to the siRNA. Nevertheless, it was found in the release study that, for LPXs, siRNA did not disassociate from DOTAP during the entire experimental process, whereas for LPNs, siRNA was released in the form of bound siRNA instead of free siRNA (Figure S1). This indicates that the interaction between siRNA and DOTAP were strong, and the siRNA might have been in the vicinity of ^{111}In-labeled lipids in the study. It can be postulated that the biodistribution patterns of ^{111}In-labeled nanoparticles observed from the SPECT study might mostly represent the biodistribution pattern of the siRNA. However, it should be acknowledged that the complicated *in vivo* environment may lead to an unexpected process.

3.4. PLGA Alleviated the Acute Inflammatory Effects of Cationic Lipid to the Lung after Intratracheal Administration. As shown in Figure 7, LPXs resulted in acute inflammatory effects to the lung, which is evidenced by the spike of IL-6 and TNF-α levels, and immune cells (i.e., macrophages and neutrophils) observed in BALF of the mice. In contrast, LPNs exhibited much mild acute inflammatory effects. The levels of IL-6 and TNF-α in BALF are similar with the PN-treated group. LPNs induced mild neutrophilia in BALF as compared to the PN-treated group, which was significantly lower than that of LPXs though. It indicates that the presence of PLGA in LPNs alleviated the acute inflammatory effects of DOTAP to the lung. Nonetheless, the higher number of macrophages induced by LPNs than the PN-treated group at 6 h after intratracheal administration suggesting that PLGA did not fully prevent the macrophage response of DOTAP. There was no eosinophil observed in the cell counts in BALF of all the tested groups in this study, which is in agreement with other studies.[54]

https://dx.doi.org/10.1021/acsami.0c21259
ACS Appl. Mater. Interfaces 2021, 13, 3722−3737

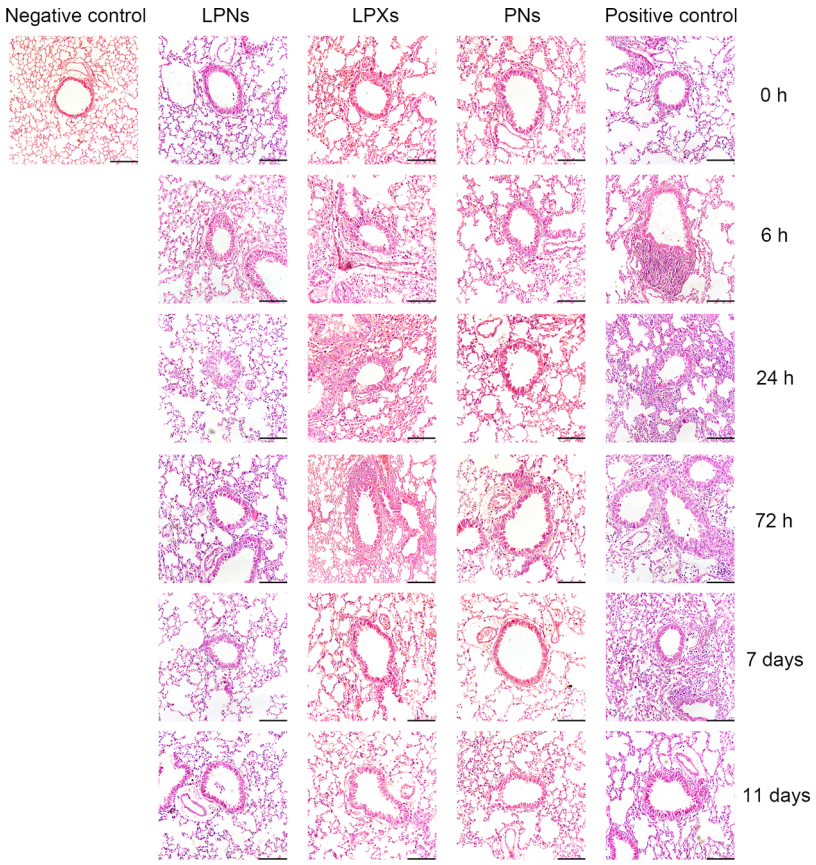

Figure 8. Histopathology images of the lung tissue treated with different nanoparticles, PBS-treated negative control, and LPS-treated positive control. Respective images of the lung tissue harvested at different time points (scale bar = 100 μm).

In addition to IL-6 and TNF-α that is related to the acute inflammatory response, other cytokines related to other immune responses in the BALF were also evaluated, including IL-1β, IFN-γ, and IL-4 (Supporting Information Figure S13). IL-1β is produced by Th1 cells, NF-κB activation,[55] and macrophage.[56] The levels of IFN-γ and IL-4 could indicate the potential of immune response.[57] The administration of LPNs resulted in an increase in IL-1β at t = 72 h but not at other sampling points (Supporting Information Figure S13A). While the administration of LPXs resulted in an increase in IL-1β and IFN-γ in BALF by t = 72 h, and the level of IFN-γ was even higher than LPS, the positive control at t = 6 h (Supporting Information Figure S13B). These results indicated the potential cause of memory T cell-related immune response by the two formulations. The presence of PLGA alleviated the potential of T cell-mediated immunity induced by DOTAP. However, the higher IFN-γ level of LPNs as compared to PNs raised a concern that the long-term presence of LPNs may induce the immune response.

The change in the total protein levels in BALF was also evaluated in this study using the BCA method, which reveals the potential of epithelial cell damage[58,59] (Supporting Information Figure S13D). The LPX group exhibit significant higher total protein levels as compared to the negative control group throughout the study, which indicated a damage in the epithelial cells. In contrast, the LPN group did not induce a significant increase in the total protein level as compared to the negative control group until 72 h. The total protein level of the LPN group on day 7 seems to be similar with that of the negative control, whereas the total protein level of LPNs on day 11 became significantly higher than that of the negative control again. This fluctuation can be attributed to the experimental deviation, nevertheless, it implies that LPNs, in long term, may induce damage to the epithelial cells. It could be attributed to the prolonged stay of LPNs in the lungs resulting in a continuous irritation to the lung (Supporting Information Figure S13D).

As a vehicle control, PNs, plain PLGA nanoparticles, were prepared with similar particle sizes (232.8 ± 7.0 nm) as that of LPNs with a zeta potential of −29.6 ± 0.4 mV and included in the biocompatibility study. The data show that PNs are very biocompatible, with similar cytokine levels, cell counts, and the total protein levels in BALF as that of the negative control. It implies LPNs induced mild irritation most likely because of the presence of DOTAP, the transfection agent, formulated in the nanoparticles. Nevertheless, a slightly higher number of immune cells than the negative control was observed on day 11 after the intratracheal administration though (Figure 7C). Although the difference in the number of the immune cells is small, a comprehensive nonclinical assessment on PNs warrant further investigation.

Histological analyses showed significant cell infiltration (macrophages and monocytes) in the lung obtained from mice treated with LPS in comparison to the mice treated with PBS at t = 6, 24, and 72 h postadministration (Figure 8). Thickening of the airway wall can be observed at t = 24 h and t = 72 h after the administration of LPXs, while slight thickening of the airway wall can be observed at t = 24 h after the administration of LPNs. The PN-treated group showed no difference in the lung tissue morphology as compared to the

https://dx.doi.org/10.1021/acsami.0c21259
ACS Appl. Mater. Interfaces 2021, 13, 3722−3737

negative control. No cell infiltration in the lung and thickening of the airway wall was observed from the mice treated with PNs in comparison to the mice with PBS treatment though.

The EE and siRNA loading of LPNs was much lower than LPXs; therefore, in order to achieve the same dose of siRNA, LPN-treated mice received higher amounts of the formulation in mass than LPX-treated mice, which raises the safety concern in the lungs. However, the presence of PLGA shielded the positive charge of DOTAP in LPNs, which alleviated the toxic effects of cationic DOTAP in the mouse lungs. LPNs still exhibited better biocompatibility than LPXs in our study, which implies that PLGA may be an excellent biocompatible polymer for pulmonary drug delivery.

4. CONCLUSIONS

This study shows that both LPXs and LPNs are able to suppress the expression of EGFP in the lungs of EGFP transgenic mice after intratracheal administration, suggesting that both nanoparticle formulations are able to transfect lung cells and exert the gene silencing effect *in vivo*. LPNs exhibit a prolonged suppression of the target protein in the lung after intratracheal administration compared to LPXs, which may be attributed to the presence of PLGA that rendered the sustained release characteristics to the nanoparticles. The presence of PLGA extended the retention of LPNs in the lung as confirmed by the SPECT/CT imaging study, which may also partially explain the difference in the duration of the pharmacological effect of the two nanoparticle formulations in the lung. In addition, the presence of PLGA in LPNs could effectively alleviate the acute inflammation effects and damage caused by DOTAP, the transfection agent, to the lung. Collectively, this study demonstrates that PLGA-based nanoparticles enable formulations to deliver siRNA drugs to mediate sustained gene silencing in the lungs after pulmonary administration, which are biocompatible and promising for clinical translation.

■ ASSOCIATED CONTENT

Supporting Information

The Supporting Information is available free of charge at https://pubs.acs.org/doi/10.1021/acsami.0c21259.

Validation of the method for determining EE in LPXs; *in vitro* release of LPNs and LPXs; establishment of A549-EGFP cell line; effects of HA on gene silencing performances of LPNs and LPXs; colloidal stability test of LPNs and LPXs; *in vitro* cell uptake study of LPNs and LPXs; genotyping of EGFP transgenic mice; comparation of transgenic mice tissue fluorescence and tissue autofluorescence; method verification of lung tissue fluorescence intensity study; images of flow cytometry study; CLSM and Western blot images of lung tissue; radiolabeling procedure and efficiency of LPNs and LPXs; SPECT/CT scanning condition and reconstruction; calculation of radioactivity; endotoxin test; and determination of cytokine levels and total protein level in BALF (PDF)

■ AUTHOR INFORMATION

Corresponding Authors

Dongmei Cun − *Wuya College of Innovation, Shenyang Pharmaceutical University, Shenyang 110016, People's Republic of China*; Phone: +86 18640041566; Email: cundongmei@163.com

Mingshi Yang − *Wuya College of Innovation, Shenyang Pharmaceutical University, Shenyang 110016, People's Republic of China; Department of Pharmacy, Faculty of Health and Medical Sciences, University of Copenhagen, Copenhagen 2100, Denmark;* orcid.org/0000-0003-3201-4696; Phone: +45 35 33 61 41; Email: mingshi.yang@sund.ku.dk

Authors

Lan Wu − *Wuya College of Innovation, Shenyang Pharmaceutical University, Shenyang 110016, People's Republic of China*

Lin-Ping Wu − *Drug Discovery Pipeline, Hefei Institute of Stem Cell and Regenerative Medicine, Guangzhou Institute of Biomedicine and Health, Chinese Academy of Sciences, Guangzhou 510530, People's Republic of China;* orcid.org/0000-0001-7579-2987

Jingya Wu − *Wuya College of Innovation, Shenyang Pharmaceutical University, Shenyang 110016, People's Republic of China*

Jin Sun − *Wuya College of Innovation, Shenyang Pharmaceutical University, Shenyang 110016, People's Republic of China;* orcid.org/0000-0001-5470-1599

Zhonggui He − *Wuya College of Innovation, Shenyang Pharmaceutical University, Shenyang 110016, People's Republic of China*

Cristina Rodríguez-Rodríguez − *Faculty of Pharmaceutical Sciences, University of British Columbia, Vancouver BC V6T 1Z3, Canada; Department of Physics & Astronomy, University of British Columbia, Vancouver BC V6T 1Z1, Canada;* orcid.org/0000-0002-3313-4422

Katayoun Saatchi − *Faculty of Pharmaceutical Sciences, University of British Columbia, Vancouver BC V6T 1Z3, Canada;* orcid.org/0000-0002-5372-6791

Lea Ann Dailey − *Department of Pharmaceutical Technology and Biopharmaceutics, University of Vienna, Vienna 1090, Austria*

Urs O. Häfeli − *Faculty of Pharmaceutical Sciences, University of British Columbia, Vancouver BC V6T 1Z3, Canada; Department of Pharmacy, Faculty of Health and Medical Sciences, University of Copenhagen, Copenhagen 2100, Denmark;* orcid.org/0000-0003-0671-4509

Complete contact information is available at: https://pubs.acs.org/10.1021/acsami.0c21259

Author Contributions

M.Y. and D.C. developed the idea. M.Y., D.C., U.O.H., K.S., and L.A.D. designed the experiments. L.W., L.-P.W., J.W., C.R.-R., and K.S. executed the experiments. L.W. wrote the original draft. M.Y., D.C., U.O.H., L.A.D., L.-P.W., J.S., and Z.H. reviewed and edited the manuscript. M.Y. and D.C. supervised the project.

Notes

The authors declare no competing financial interest.

■ ACKNOWLEDGMENTS

We acknowledge the National Natural Science Foundation of China (no. 81573380) and Liaoning Pan Deng Xue Zhe Scholarship for the financial support. This study was further supported by the Lundbeck Foundation, Denmark (grant no.

2014-4176, the UBC-SUND Lundbeck Foundation professorship to U.O.H.). This article is based upon work from COST Action MP1404 SimInhale "Simulation and pharmaceutical technologies for advanced patient-tailored inhaled medicines", supported by COST (European Cooperation in Science and Technology). In addition, D.C. would like to acknowledge the financial support of the Guiding Project for Science and Technology of Liaoning Province (no. 2019-ZD-0448). Also L.-P.W. acknowledges financial support from National Key R&D Program of China (no. 2019YFA0110501), International Science and Technology Cooperation Program of Guangdong Province (no. 2019A050510028), International Science and Technology Cooperation Project of HuangPu, Guangzhou City (no. 2018GH15), and National Science and Technology Major Projects for New Drug Development (no. 2018ZX09733-006). The authors would also like to thank Canada Foundation for Innovation (Project No. 25413) for its support of the imaging facility (http://invivoimaging.ca/). We are very grateful to Prof. Dr. Camilla Foged at the Department of Pharmacy, University of Copenhagen for providing her critical comments to improve the manuscript. We are also very thankful to Prof. Dr. Yongkui Jing at Wuya College of Innovation, Shenyang Pharmaceutical University for supporting the cell study.

■ ABBREVIATIONS

siRNA, small interfering RNA
EGFP, enhanced green fluorescent protein
DOTAP, 1,2-dioleoyl-3-trimethylammonium-propane
PLGA, poly(lactide-*co*-glycolide)
LPNs, lipid-polymer hybrid nanoparticles
SPECT/CT, single-photon emission computed tomography/computed tomography
RNAi, RNA interference
ITLC, instant thin-layer chromatography

■ REFERENCES

(1) Merkel, O. M.; Rubinstein, I.; Kissel, T. Sirna Delivery to the Lung: What's New? *Adv. Drug Deliv. Rev.* **2014**, *75*, 112−128.
(2) de Fougerolles, A.; Novobrantseva, T. Sirna and the Lung: Research Tool or Therapeutic Drug? *Curr. Opin. Pharmacol.* **2008**, *8*, 280−285.
(3) Solomon, S. D.; Adams, D.; Kristen, A.; Grogan, M.; González-Duarte, A.; Maurer, M. S.; Merlini, G.; Damy, T.; Slama, M. S.; Brannagan, T. H.; Dispenzieri, A.; Berk, J. L.; Shah, A. M.; Garg, P.; Vaishnaw, A.; Karsten, V.; Chen, J.; Gollob, J.; Vest, J.; Suhr, O. Effects of Patisiran, an Rna Interference Therapeutic, on Cardiac Parameters in Patients with Hereditary Transthyretin-Mediated Amyloidosis. *Circulation* **2019**, *139*, 431−443.
(4) Watts, J.; Deleavey, G.; Damha, M. Chemically Modified Sirna: Tools and Applications. *Drug Discov. Today* **2008**, *13*, 842−855.
(5) Mainelis, G.; Seshadri, S.; Garbuzenko, O. B.; Han, T.; Wang, Z.; Minko, T. Characterization and Application of a Nose-Only Exposure Chamber for Inhalation Delivery of Liposomal Drugs and Nucleic Acids to Mice. *J. Aerosol Med. Pulm. Drug Delivery* **2013**, *26*, 345−354.
(6) Taratula, O.; Kuzmov, A.; Shah, M.; Garbuzenko, O. B.; Minko, T. Nanostructured Lipid Carriers as Multifunctional Nanomedicine Platform for Pulmonary Co-Delivery of Anticancer Drugs and Sirna. *J. Controlled Release* **2013**, *171*, 349−357.
(7) Beyerle, A.; Braun, A.; Merkel, O.; Koch, F.; Kissel, T.; Stoeger, T. Comparative in Vivo Study of Poly(Ethylene Imine)/Sirna Complexes for Pulmonary Delivery in Mice. *J. Controlled Release* **2011**, *151*, 51−56.
(8) Kaminskas, L. M.; McLeod, V. M.; Ryan, G. M.; Kelly, B. D.; Haynes, J. M.; Williamson, M.; Thienthong, N.; Owen, D. J.; Porter, C. J. H. Pulmonary Administration of a Doxorubicin-Conjugated Dendrimer Enhances Drug Exposure to Lung Metastases and Improves Cancer Therapy. *J. Controlled Release* **2014**, *183*, 18−26.
(9) Frede, A.; Neuhaus, B.; Knuschke, T.; Wadwa, M.; Kollenda, S.; Klopfleisch, R.; Hansen, W.; Buer, J.; Bruder, D.; Epple, M.; Westendorf, A. M. Local Delivery of Sirna-Loaded Calcium Phosphate Nanoparticles Abates Pulmonary Inflammation. *Nanomedicine* **2017**, *13*, 2395−2403.
(10) Kulkarni, J. A.; Witzigmann, D.; Chen, S.; Cullis, P. R.; van der Meel, R. Lipid Nanoparticle Technology for Clinical Translation of Sirna Therapeutics. *Acc. Chem. Res.* **2019**, *52*, 2435−2444.
(11) Gilleron, J.; Querbes, W.; Zeigerer, A.; Borodovsky, A.; Marsico, G.; Schubert, U.; Manygoats, K.; Seifert, S.; Andree, C.; Stöter, M.; Epstein-Barash, H.; Zhang, L.; Koteliansky, V.; Fitzgerald, K.; Fava, E.; Bickle, M.; Kalaidzidis, Y.; Akinc, A.; Maier, M.; Zerial, M. Image-Based Analysis of Lipid Nanoparticle−Mediated Sirna Delivery, Intracellular Trafficking and Endosomal Escape. *Nat. Biotechnol.* **2013**, *31*, 638−646.
(12) Thanki, K.; Zeng, X.; Justesen, S.; Tejlmann, S.; Falkenberg, E.; Van Driessche, E.; Mørck Nielsen, H.; Franzyk, H.; Foged, C. Engineering of Small Interfering Rna-Loaded Lipidoid-Poly(Dl-Lactic-Co-Glycolic Acid) Hybrid Nanoparticles for Highly Efficient and Safe Gene Silencing: A Quality by Design-Based Approach. *Eur. J. Pharm. Biopharm.* **2017**, *120*, 22−33.
(13) André, E. M.; Pensado, A.; Resnier, P.; Braz, L.; Rosa da Costa, A. M.; Passirani, C.; Sanchez, A.; Montero-Menei, C. N. Characterization and Comparison of Two Novel Nanosystems Associated with Sirna for Cellular Therapy. *Int. J. Pharm.* **2016**, *497*, 255−267.
(14) te Boekhorst, B. C. M.; Jensen, L. B.; Colombo, S.; Varkouhi, A. K.; Schiffelers, R. M.; Lammers, T.; Storm, G.; Nielsen, H. M.; Strijkers, G. J.; Foged, C.; Nicolay, K. Mri-Assessed Therapeutic Effects of Locally Administered Plga Nanoparticles Loaded with Anti-Inflammatory Sirna in a Murine Arthritis Model. *J. Controlled Release* **2012**, *161*, 772−780.
(15) Cun, D.; Jensen, D. K.; Maltesen, M. J.; Bunker, M.; Whiteside, P.; Scurr, D.; Foged, C.; Nielsen, H. M. High Loading Efficiency and Sustained Release of Sirna Encapsulated in Plga Nanoparticles: Quality by Design Optimization and Characterization. *Eur. J. Pharm. Biopharm.* **2011**, *77*, 26−35.
(16) Colombo, S.; Cun, D.; Remaut, K.; Bunker, M.; Zhang, J.; Martin-Bertelsen, B.; Yaghmur, A.; Braeckmans, K.; Nielsen, H. M.; Foged, C. Mechanistic Profiling of the Sirna Delivery Dynamics of Lipid−Polymer Hybrid Nanoparticles. *J. Controlled Release* **2015**, *201*, 22−31.
(17) Lu, Y.; Liu, L.; Wang, Y.; Li, F.; Zhang, J.; Ye, M.; Zhao, H.; Zhang, X.; Zhang, M.; Zhao, J.; Yan, B.; Yang, A.; Feng, H.; Zhang, R.; Ren, X. Sirna Delivered by Egfr-Specific Scfv Sensitizes Egfr-Tki-Resistant Human Lung Cancer Cells. *Biomaterials* **2016**, *76*, 196−207.
(18) Chen, G.; Kronenberger, P.; Teugels, E.; Umelo, I. A.; De Grève, J. Effect of Sirnas Targeting the Egfr T790m Mutation in a Non-Small Cell Lung Cancer Cell Line Resistant to Egfr Tyrosine Kinase Inhibitors and Combination with Various Agents. *Biochem. Biophys. Res. Commun.* **2013**, *431*, 623−629.
(19) Zhang, Y.; Schwerbrock, N. M.; Rogers, A. B.; Kim, W. Y.; Huang, L. Codelivery of Vegf Sirna and Gemcitabine Monophosphate in a Single Nanoparticle Formulation for Effective Treatment of Nsclc. *Mol. Ther.* **2013**, *21*, 1559−1569.
(20) Bitko, V.; Musiyenko, A.; Shulyayeva, O.; Barik, S. Inhibition of Respiratory Viruses by Nasally Administered Sirna. *Nat. Med.* **2005**, *11*, 50−55.
(21) Yu, K.; Deng, S.; Wang, H.; Zhang, Y.; Chen, X.; Wang, K.; Hu, R.; Lian, Z.; Li, N. Small Interfering Rna Expression Inhibits Avian Infectious Bronchitis Virus Replication and Inflammatory Response. *Antivir. Ther.* **2016**, *21*, 469−479.
(22) Clark, K. L.; Hughes, S. A.; Bulsara, P.; Coates, J.; Moores, K.; Parry, J.; Carr, M.; Mayer, R. J.; Wilson, P.; Gruenloh, C.; Levin, D.; Darton, J.; Weber, W.-M.; Sobczak, K.; Gill, D. R.; Hyde, S. C.; Davies, L. A.; Pringle, I. A.; Sumner-Jones, S. G.; Jadhav, V.; Jamison, S.; Strapps, W. R.; Pickering, V.; Edbrooke, M. R. Pharmacological

https://dx.doi.org/10.1021/acsami.0c21259
ACS Appl. Mater. Interfaces 2021, 13, 3722−3737

Characterization of a Novel Enacα Sirna (Gsk2225745) with Potential for the Treatment of Cystic Fibrosis. *Mol. Ther. Nucleic Acids* **2013**, *2*, No. e65.
(23) Huang, H.-Y.; Lee, C.-C.; Chiang, B.-L. Small Interfering Rna against Interleukin-5 Decreases Airway Eosinophilia and Hyper-Responsiveness. *Gene Ther.* **2008**, *15*, 660−667.
(24) Lee, C.-C.; Huang, H.-Y.; Chiang, B.-L. Lentiviral-Mediated Gata-3 Rnai Decreases Allergic Airway Inflammation and Hyper-responsiveness. *Mol. Ther.* **2008**, *16*, 60−65.
(25) Wu, L.; Zhang, J.; Qu, J. M.; Bai, C.-x.; Merrilees, M. Deposition of Insoluble Elastin by Pulmonary Fibroblasts from Patients with Copd Is Increased by Treatment with Versican Sirna. *Int. J. Chronic Obstr. Pulm. Dis.* **2017**, *12*, 267−273.
(26) Rose, S. D.; Kim, D. H.; Amarzguioui, M.; Heidel, J. D.; Collingwood, M. A.; Davis, M. E.; Rossi, J. J.; Behlke, M. A. Functional Polarity Is Introduced by Dicer Processing of Short Substrate Rnas. *Nucleic Acids Res.* **2005**, *33*, 4140−4156.
(27) Li, Y.; Cheng, Q.; Jiang, Q.; Huang, Y.; Liu, H.; Zhao, Y.; Cao, W.; Ma, G.; Dai, F.; Liang, X.; Liang, Z.; Zhang, X. Enhanced Endosomal/Lysosomal Escape by Distearoyl Phosphoethanolamine-Polycarboxybetaine Lipid for Systemic Delivery of Sirna. *J. Controlled Release* **2014**, *176*, 104−114.
(28) Jensen, D. K.; Jensen, L. B.; Koocheki, S.; Bengtson, L.; Cun, D.; Nielsen, H. M.; Foged, C. Design of an Inhalable Dry Powder Formulation of Dotap-Modified Plga Nanoparticles Loaded with Sirna. *J. Controlled Release* **2012**, *157*, 141−148.
(29) Huang, Z.; Huang, Y.; Ma, C.; Ma, X.; Zhang, X.; Lin, L.; Zhao, Z.; Pan, X.; Wu, C. Endotracheal Aerosolization Device for Laboratory Investigation of Pulmonary Delivery of Nanoparticle Suspensions: In Vitro and in Vivo Validation. *Mol. Pharm.* **2018**, *15*, 5521−5533.
(30) Ikawa, M.; Kominami, K.; Yoshimura, Y.; Tanaka, K.; Nishimune, Y.; Okabe, M. Green Fluorescent Protein as a Marker in Transgenic Mice. *Dev., Growth Differ.* **1995**, *37*, 455−459.
(31) Pathak, A.; Kumar, P.; Chuttani, K.; Jain, S.; Mishra, A. K.; Vyas, S. P.; Gupta, K. C. Gene Expression, Biodistribution, and Pharmacoscintigraphic Evaluation of Chondroitin Sulfate−Pei Nanoconstructs Mediated Tumor Gene Therapy. *ACS Nano* **2009**, *3*, 1493−1505.
(32) Loening, A. M.; Gambhir, S. S. Amide: A Free Software Tool for Multimodality Medical Image Analysis. *Mol. Imag.* **2003**, *2*, 131−137.
(33) Jaiprasart, P.; Yeung, B. Z.; Lu, Z.; Wientjes, M. G.; Cui, M.; Hsieh, C.-M.; Woo, S.; Au, J. L.-S. Quantitative Contributions of Processes by Which Polyanion Drugs Reduce Intracellular Bioavailability and Transfection Efficiency of Cationic Sirna Lipoplex. *J. Controlled Release* **2018**, *270*, 101−113.
(34) Kasai, H.; Inoue, K.; Imamura, K.; Yuvienco, C.; Montclare, J. K.; Yamano, S. Efficient Sirna Delivery and Gene Silencing Using a Lipopolypeptide Hybrid Vector Mediated by a Caveolae-Mediated and Temperature-Dependent Endocytic Pathway. *J. Nanobiotechnol.* **2019**, *17*, 11.
(35) Dehousse, V.; Garbacki, N.; Jaspart, S.; Castagne, D.; Piel, G.; Colige, A.; Evrard, B. Comparison of Chitosan/Sirna and Trimethylchitosan/Sirna Complexes Behaviour in Vitro. *Int. J. Biol. Macromol.* **2010**, *46*, 342−349.
(36) Hickerson, R. P.; Vlassov, A. V.; Wang, Q.; Leake, D.; Ilves, H.; Gonzalez-Gonzalez, E.; Contag, C. H.; Johnston, B. H.; Kaspar, R. L. Stability Study of Unmodified Sirna and Relevance to Clinical Use. *Oligonucleotides* **2008**, *18*, 345−354.
(37) Merkel, O. M.; Beyerle, A.; Librizzi, D.; Pfestroff, A.; Behr, T. M.; Sproat, B.; Barth, P. J.; Kissel, T. Nonviral Sirna Delivery to the Lung: Investigation of Peg−Pei Polyplexes and Their in Vivo Performance. *Mol. Pharm.* **2009**, *6*, 1246−1260.
(38) Nielsen, E. J. B.; Nielsen, J. M.; Becker, D.; Karlas, A.; Prakash, H.; Glud, S. Z.; Merrison, J.; Besenbacher, F.; Meyer, T. F.; Kjems, J.; Howard, K. A. Pulmonary Gene Silencing in Transgenic Egfp Mice Using Aerosolised Chitosan/Sirna Nanoparticles. *Pharm. Res.* **2010**, *27*, 2520−2527.
(39) Pinese, C.; Lin, J.; Milbreta, U.; Li, M.; Wang, Y.; Leong, K. W.; Chew, S. Y. Sustained Delivery of Sirna/Mesoporous Silica Nanoparticle Complexes from Nanofiber Scaffolds for Long-Term Gene Silencing. *Acta Biomater.* **2018**, *76*, 164−177.
(40) Luo, J.; Höhn, M.; Reinhard, S.; Loy, D. M.; Klein, P. M.; Wagner, E. Il4-Receptor-Targeted Dual Antitumoral Apoptotic Peptide—Sirna Conjugate Lipoplexes. *Adv. Funct. Mater.* **2019**, *29*, 1900697.
(41) Yi, D.; Naqwi, A.; Panoskaltsis-Mortari, A.; Wiedmann, T. S. Distribution of Aerosols in Mouse Lobes by Fluorescent Imaging. *Int. J. Pharm.* **2012**, *426*, 108−115.
(42) Tonnis, W. F.; Bagerman, M.; Weij, M.; Sjollema, J.; Frijlink, H. W.; Hinrichs, W. L. J.; de Boer, A. H. A Novel Aerosol Generator for Homogenous Distribution of Powder over the Lungs after Pulmonary Administration to Small Laboratory Animals. *Eur. J. Pharm. Biopharm.* **2014**, *88*, 1056−1063.
(43) Duret, C.; Wauthoz, N.; Merlos, R.; Goole, J.; Maris, C.; Roland, I.; Sebti, T.; Vanderbist, F.; Amighi, K. In Vitro and in Vivo Evaluation of a Dry Powder Endotracheal Insufflator Device for Use in Dose-Dependent Preclinical Studies in Mice. *Eur. J. Pharm. Biopharm.* **2012**, *81*, 627−634.
(44) Wu, L.; Rodríguez-Rodríguez, C.; Cun, D.; Yang, M.; Saatchi, K.; Häfeli, U. O. Quantitative Comparison of Three Widely-Used Pulmonary Administration Methods in Vivo with Radiolabeled Inhalable Nanoparticles. *Eur. J. Pharm. Biopharm.* **2020**, *152*, 108−115.
(45) Okuda, T.; Morishita, M.; Mizutani, K.; Shibayama, A.; Okazaki, M.; Okamoto, H. Development of Spray-Freeze-Dried Sirna/Pei Powder for Inhalation with High Aerosol Performance and Strong Pulmonary Gene Silencing Activity. *J. Controlled Release* **2018**, *279*, 99−113.
(46) Thanki, K.; van Eetvelde, D.; Geyer, A.; Fraire, J.; Hendrix, R.; Van Eygen, H.; Putteman, E.; Sami, H.; de Souza Carvalho-Wodarz, C.; Franzyk, H.; Nielsen, H. M.; Braeckmans, K.; Lehr, C.-M.; Ogris, M.; Foged, C. Mechanistic Profiling of the Release Kinetics of Sirna from Lipidoid-Polymer Hybrid Nanoparticles in Vitro and in Vivo after Pulmonary Administration. *J. Controlled Release* **2019**, *310*, 82−93.
(47) Oh, N.; Park, J.-H. Endocytosis and Exocytosis of Nanoparticles in Mammalian Cells. *Int. J. Nanomed.* **2014**, *9*, 51−63.
(48) Patel, B.; Gupta, N.; Ahsan, F. Particle Engineering to Enhance or Lessen Particle Uptake by Alveolar Macrophages and to Influence the Therapeutic Outcome. *Eur. J. Pharm. Biopharm.* **2015**, *89*, 163−174.
(49) Beck-Broichsitter, M.; Merkel, O. M.; Kissel, T. Controlled Pulmonary Drug and Gene Delivery Using Polymeric Nano-Carriers. *J. Controlled Release* **2012**, *161*, 214−224.
(50) Huang, Z.; Huang, Y.; Wang, W.; Fu, F.; Wang, W.; Dang, S.; Li, C.; Ma, C.; Zhang, X.; Zhao, Z.; Pan, X.; Wu, C. Relationship between Particle Size and Lung Retention Time of Intact Solid Lipid Nanoparticle Suspensions after Pulmonary Delivery. *J. Controlled Release* **2020**, *325*, 206−222.
(51) Braakhuis, H. M.; Gosens, I.; Krystek, P.; Boere, J. A. F.; Cassee, F. R.; Fokkens, P. H. B.; Post, J. A.; van Loveren, H.; Park, M. V. D. Z. Particle Size Dependent Deposition and Pulmonary Inflammation after Short-Term Inhalation of Silver Nanoparticles. *Part. Fibre Toxicol.* **2014**, *11*, 49.
(52) Haque, S.; Whittaker, M.; McIntosh, M. P.; Pouton, C. W.; Phipps, S.; Kaminskas, L. M. A Comparison of the Lung Clearance Kinetics of Solid Lipid Nanoparticles and Liposomes by Following the 3h-Labelled Structural Lipids after Pulmonary Delivery in Rats. *Eur. J. Pharm. Biopharm.* **2018**, *125*, 1−12.
(53) Ryan, G. M.; Kaminskas, L. M.; Kelly, B. D.; Owen, D. J.; McIntosh, M. P.; Porter, C. J. H. Pulmonary Administration of Pegylated Polylysine Dendrimers: Absorption from the Lung Versus Retention within the Lung Is Highly Size-Dependent. *Mol. Pharm.* **2013**, *10*, 2986−2995.
(54) Woods, A.; Patel, A.; Spina, D.; Riffo-Vasquez, Y.; Babin-Morgan, A.; de Rosales, R. T. M.; Sunassee, K.; Clark, S.; Collins, H.;

https://dx.doi.org/10.1021/acsami.0c21259
ACS Appl. Mater. Interfaces 2021, 13, 3722−3737

Bruce, K.; Dailey, L. A.; Forbes, B. In Vivo Biocompatibility, Clearance, and Biodistribution of Albumin Vehicles for Pulmonary Drug Delivery. *J. Controlled Release* **2015**, *210*, 1−9.
(55) Ribeiro, A.; Almeida, V. I.; Costola-de-Souza, C.; Ferraz-de-Paula, V.; Pinheiro, M. L.; Vitoretti, L. B.; Gimenes-Junior, J. A.; Akamine, A. T.; Crippa, J. A.; Tavares-de-Lima, W.; Palermo-Neto, J. Cannabidiol Improves Lung Function and Inflammation in Mice Submitted to Lps-Induced Acute Lung Injury. *Immunopharmacol. Immunotoxicol.* **2015**, *37*, 35−41.
(56) Haque, S.; Feeney, O.; Meeusen, E.; Boyd, B. J.; McIntosh, M. P.; Pouton, C. W.; Whittaker, M.; Kaminskas, L. M. Local Inflammation Alters the Lung Disposition of a Drug Loaded Pegylated Liposome after Pulmonary Dosing to Rats. *J. Controlled Release* **2019**, *307*, 32−43.
(57) Dwivedi, V.; Manickam, C.; Binjawadagi, B.; Renukaradhya, G. J. Plga Nanoparticle Entrapped Killed Porcine Reproductive and Respiratory Syndrome Virus Vaccine Helps in Viral Clearance in Pigs. *Vet. Microbiol.* **2013**, *166*, 47−58.
(58) Jones, M.-C.; Jones, S. A.; Riffo-Vasquez, Y.; Spina, D.; Hoffman, E.; Morgan, A.; Patel, A.; Page, C.; Forbes, B.; Dailey, L. A. Quantitative Assessment of Nanoparticle Surface Hydrophobicity and Its Influence on Pulmonary Biocompatibility. *J. Controlled Release* **2014**, *183*, 94−104.
(59) Dailey, L. A.; Jekel, N.; Fink, L.; Gessler, T.; Schmehl, T.; Wittmar, M.; Kissel, T.; Seeger, W. Investigation of the Proinflammatory Potential of Biodegradable Nanoparticle Drug Delivery Systems in the Lung. *Toxicol. Appl. Pharmacol.* **2006**, *215*, 100−108.

https://dx.doi.org/10.1021/acsami.0c21259
ACS Appl. Mater. Interfaces 2021, 13, 3722−3737